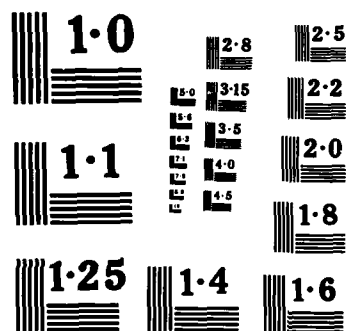


ANALYSIS AND MODEL/DATA COMPARISONS OF LARGE-SCALE  
RELEASES OF NITROGEN TETROXIDE(U) LAWRENCE LIVERMORE  
NATIONAL LAB CA T G MCRAE JUN 85 UCID-20388  
AFESC/ESL-TR-85-86 W-7405-ENG-48 F/G 14/2

NL

F/G 14/2

DTIC



NATIONAL BUREAU OF STANDARDS  
MICROCOPY RESOLUTION TEST CHART

AD-A158 752

ESL-TR-85-06

①

# Analysis and Model/Data Comparisons of Large-Scale Releases of Nitrogen Tetroxide

THOMAS G. McRAE  
LAWRENCE LIVERMORE NATIONAL LABORATORY  
LIVERMORE, CALIFORNIA 94550

JUNE 1985

FINAL REPORT

JUNE 1983 - SEPTEMBER 1984

DTIC  
ELECTE  
S SEP 3 1985 D  
B

APPROVED FOR PUBLIC RELEASE: DISTRIBUTION UNLIMITED



ENGINEERING & SERVICES LABORATORY  
AIR FORCE ENGINEERING & SERVICES CENTER  
TYNDALL AIR FORCE BASE, FLORIDA 32403

85 8 29 066

FILE COPY

NOTICE

PLEASE DO NOT REQUEST COPIES OF THIS REPORT FROM  
HQ AFESC/RD (ENGINEERING AND SERVICES LABORATORY).  
ADDITIONAL COPIES MAY BE PURCHASED FROM:

NATIONAL TECHNICAL INFORMATION SERVICE  
5285 PORT ROYAL ROAD  
SPRINGFIELD, VIRGINIA 22161

FEDERAL GOVERNMENT AGENCIES AND THEIR CONTRACTORS  
REGISTERED WITH DEFENSE TECHNICAL INFORMATION CENTER  
SHOULD DIRECT REQUESTS FOR COPIES OF THIS REPORT TO:

DEFENSE TECHNICAL INFORMATION CENTER  
CAMERON STATION  
ALEXANDRIA, VIRGINIA 22314

UNCLASSIFIED

SECURITY CLASSIFICATION OF THIS PAGE

## REPORT DOCUMENTATION PAGE

1a. REPORT SECURITY CLASSIFICATION UNCLASSIFIED			1b. RESTRICTIVE MARKINGS		
2a. SECURITY CLASSIFICATION AUTHORITY			3. DISTRIBUTION/AVAILABILITY OF REPORT Approved for public release; distribution unlimited		
2b. DECLASSIFICATION/DOWNGRADING SCHEDULE					
4. PERFORMING ORGANIZATION REPORT NUMBER(S)  UCID 20388			5. MONITORING ORGANIZATION REPORT NUMBER(S)  ESL - TR- 85-06		
6a. NAME OF PERFORMING ORGANIZATION Lawrence Livermore National Laboratory		6b. OFFICE SYMBOL (If applicable)	7a. NAME OF MONITORING ORGANIZATION HQ AFESC/RDV		
6c. ADDRESS (City, State and ZIP Code) Livermore, California 94550			7b. ADDRESS (City, State and ZIP Code) Tyndall AFB FL 32403		
8a. NAME OF FUNDING/SPONSORING ORGANIZATION		8b. OFFICE SYMBOL (If applicable)	9. PROCUREMENT INSTRUMENT IDENTIFICATION NUMBER W-7405-ENG-48		
8c. ADDRESS (City, State and ZIP Code)			10. SOURCE OF FUNDING NOS.		
			PROGRAM ELEMENT NO. 64708F	PROJECT NO. 2054	TASK NO. 30
11. TITLE (Include Security Classification) Analysis and Model/ Data Comparisons of Large-Scale Releases of Nitrogen Tetroxide					
12. PERSONAL AUTHOR(S) Thomas G. McRae					
13a. TYPE OF REPORT Final		13b. TIME COVERED FROM Jun 83 TO Sep 84		14. DATE OF REPORT (Yr., Mo., Day) June 1985	
15. PAGE COUNT 74					
16. SUPPLEMENTARY NOTATION Availability of this report is specified on reverse of front cover.					
17. COSATI CODES			18. SUBJECT TERMS (Continue on reverse if necessary and identify by block number)		
FIELD	GROUP	SUB. GR.	Nitrogen Tetroxide Model Comparison		
04	01		Source Strength Model Evaporation Models		
04	02		Heavy-gas Dispersion Dispersion Models		
19. ABSTRACT (Continue on reverse if necessary and identify by block number) Cum During the fall of 1983, the Lawrence Livermore National Laboratory (LLNL) conducted a series of large-scale (3-5m <sup>3</sup> ) nitrogen tetroxide (N <sub>2</sub> O <sub>4</sub> ) spill tests for the U.S. Air Force Engineering and Services Laboratory (ESL), Tyndall AFB, FL. The purpose of the test series was to determine the source strength characteristics and heavy-gas dispersion aspects of large N <sub>2</sub> O <sub>4</sub> spills. Six N <sub>2</sub> O <sub>4</sub> spill tests were accomplished. Four tests were for the purpose of dispersion and source strength studies and two tests for evaluation of a Portable Foam Vapor Suppression System.  The source strength and downwind dispersion results of two of the spill tests are used to evaluate several source strength and dispersion models. The experiments and diagnostic procedures are briefly described. Source strength estimates from two of the tests are compared with those predicted by the Ille and Springer Model, the Shell evaporation model, the Army model, the ESL model, and the Air Weather Service model. One conclusion from					
20. DISTRIBUTION/AVAILABILITY OF ABSTRACT UNCLASSIFIED/UNLIMITED <input checked="" type="checkbox"/> SAME AS RPT. <input type="checkbox"/> DTIC USERS <input type="checkbox"/>			21. ABSTRACT SECURITY CLASSIFICATION UNCLASSIFIED		
22a. NAME OF RESPONSIBLE INDIVIDUAL LAWRENCE E. KEY, Capt, USAF			22b. TELEPHONE NUMBER (Include Area Code) (904) 283-4234		22c. OFFICE SYMBOL HQ AFESC/RDVS

DD FORM 1473, 83 APR

EDITION OF 1 JAN 73 IS OBSOLETE.

UNCLASSIFIED  
SECURITY CLASSIFICATION OF THIS PAGE

Block 19 continued

these source strength comparisons is that the internal energy (evaporative cooling) heat source is a major contributor to the source strength. The comparison also demonstrates that source strength models need improvement. Current models appear to overestimate the importance of windspeed and underestimate the importance of evaporative cooling, liquid depth, and soil seepage.

The primary purpose of the Eagle test series was to demonstrate the heavy-gas dispersion aspect of large-scale releases of  $N_2O_4$  vapors. The denser-than-air character of a heavy-gas cloud affects its subsequent dispersion in two main ways. The greater inertia of the heavy gas tends to reduce the rate of turbulent mixing from that of a trace gas and thereby reduces the growth of the cloud. The greater density of the cloud produces a gravity flow or slumping which tends to reduce the cloud height and increase its width. This report describes four simple dispersion models and compares model predictions with the results of two of the spill tests. The four models used in this study are the Ocean Breeze/Dry Gulch model, the Pasquill-Hanna Gaussian Plume model, the Shell dispersion model, and the CHARM model. The model comparison results indicate that all of the models examined substantially underpredict the measured peak downwind gas concentration by factors ranging from 2 to 14 depending upon the various assumptions employed. The parameters used in the simple models are based on long-averaging times and therefore include large-scale meander effects. These are inappropriate for predicting short term concentrations. In addition, the cloud-spreading parameters for heavier-than-air releases are different than those of trace gases. Measured cloud height, for instance, is only 0.3 to 0.1 that predicted by the simple models.



Accession For	
NTIS GRA&I	<input checked="" type="checkbox"/>
DTIC TAB	<input type="checkbox"/>
Unannounced	<input type="checkbox"/>
Justification	
By	
Distribution/	
Availability Codes	
Dist	Avail and/or Special
A-1	

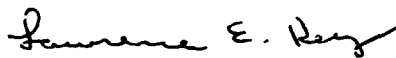
## PREFACE

This report was prepared by Lawrence Livermore National Laboratory (LLNL), Post Office Box 808, Livermore California 94550, under contract W-7405-ENG-48, for the Air Force Engineering and Services Center, Engineering and Services Laboratory (AFESC/RDVS), Tyndall Air Force Base, Florida 32403.


The report summarizes work done between June 1983 and September 1984. The principal investigator at LLNL was Thomas G. McRae. Major Gary G. Worley and Captain Lawrence E. Key were the AFESC/RDVS project officers.

This report has been reviewed by the Public Affairs Office (PA) and is releasable to the National Technical Information Service (NTIS). At NTIS it will be available to the general public, including foreign nationals.

This technical report has been reviewed and is approved for publication.



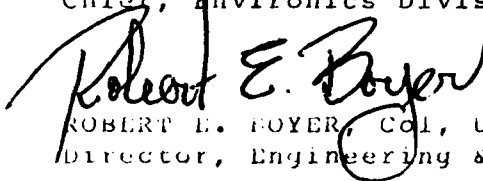
LAWRENCE E. KEY, Capt, USAF



F. THOMAS LUBOZYNSKI, Maj, USAF, BSC  
Senior Research Meteorologist Chief, Environmental Sciences Branch



ROBERT F. OLFENBUTTEL, Lt Col, USAF, BSC  
Chief, Environics Division



ROBERT E. BOYER, Col, USAF  
Director, Engineering & Services Laboratory

# TABLE OF CONTENTS

Section	Page
I INTRODUCTION . . . . .	1
II EXPERIMENT DESCRIPTION . . . . .	3
A. FACILITY AND OPERATION . . . . .	3
B. THE DIAGNOSTIC SYSTEM. . . . .	6
III SOURCE STRENGTH RESULTS . . . . .	12
A. THE SPILL AREA HEAT SOURCE APPROACH. . . . .	15
1. The Eagle 3 Test . . . . .	16
2. The Eagle 6 Test . . . . .	20
B. THE MIST FORMATION APPROACH . . . . .	24
C. THE EAGLE 3 AND EAGLE 6 SOURCE STRENGTHS . . . . .	29
D. SOURCE STRENGTH DATA OF PREVIOUS TESTS . . . . .	30
1. The Edwards AFB Tests . . . . .	30
2. The Edgewood Arsenal Tests . . . . .	32
E. COMPARISON OF EAGLE RESULTS WITH SOURCE STRENGTH MODEL PREDICTIONS . . . . .	33
1. The Ille and Springer Model . . . . .	34
2. The Shell Evaporation Model . . . . .	34
3. The Army Model . . . . .	35
4. The ESL Model . . . . .	36
5. The AWS Model . . . . .	36
F. SUMMARY AND DISCUSSION OF SOURCE STRENGTH RESULTS . . . . .	36
1. Experimental Comparisons . . . . .	37
2. Model Comparisons . . . . .	39
IV VAPOR CLOUD DISPERSION RESULTS . . . . .	41
A. NO <sub>2</sub> DOWNWIND DATA ANALYSIS . . . . .	41
1. The Eagle 3 Test . . . . .	43
2. The Eagle 6 Test . . . . .	50
B. COMPARISON OF DATA WITH DISPERSION MODEL PREDICTIONS. . . . .	55
1. The OB/DG Model . . . . .	55
2. The Pasquill-Hanna Gaussian Plume Model . . . . .	57
3. The Shell Dispersion Model. . . . .	62
4. The CHARM Model . . . . .	63



# TABLE OF CONTENTS (CONTINUED)

Section	Page
C. SUMMARY OF DISPERSION RESULTS. . . . .	64
V CONCLUSIONS . . . . .	66
A. N <sub>2</sub> O <sub>4</sub> SOURCE STRENGTH CONCLUSIONS . . . . .	66
B. N <sub>2</sub> O <sub>4</sub> VAPOR DISPERSION CONCLUSIONS . . . . .	67
REFERENCES . . . . .	68

# LIST OF FIGURES

Figure	Title	Page
1	Eagle Series Spill Facility Site Layout . . . . .	4
2	Eagle Series Spill Configurations . . . . .	5
3	Eagle Series Diagnostic Systems. . . . .	8
4	Eagle 3 Spill Area Heat Source Data . . . . .	17
5	Eagle 3 Spill Area Source Strength Components . . . . .	19
6	Eagle 3 Source Strength Estimate Using the Spill Area Heat Source Approach . . . . .	21
7	Eagle 6 Spill Area Source Strength Components . . . . .	22
8	Eagle 6 Source Strength Estimate Using the Spill Area Heat Source Approach . . . . .	23
9	$N_2O_4$ + $NO_2$ Vapor Flux at 25 meters for the Eagle 3 and Eagle 6 Spills . . . . .	25
10	Eagle 3 and Eagle 6 Source Strength Estimates Using the Mist Formation Approach . . . . .	28
11	The Eagle 3 $NO_2$ Concentration Data (1 meter high, 785 meters downwind) . . . . .	44
12	Eagle 3 Cloud Centerline Trajectories. . . . .	46
13	Eagle 3 Crosswind $NO_2$ Concentration Contours at $t = 300$ seconds (785 meters downwind). . . . .	47
14	The Gaussian Equivalent Crosswind Concentration Distribution for the Eagle 3 Data at 785 m . . . . .	49
15	The Eagle 6 $NO_2$ Concentration Data (1 meter high, 785 meters downwind). . . . .	51
16	Eagle 6 Cloud Centerline Trajectories. . . . .	52
17	Eagle 6 Crosswind $NO_2$ Concentration Contours at $t = 430$ seconds (785 meters downwind). . . . .	53
18	Gaussian Equivalent Crosswind Concentration Distribution for the Eagle 6 Data at 785 meters . . . . .	54
19	Variation of $\sigma_y$ at 12 meters with Averaging Time Period for the Eagle 3 and Eagle 6 Tests. . . . .	59
20	Eagle 3 and Eagle 6 Crosswind Concentrations as Predicted by the Gaussian Plume Model. . . . .	61

# LIST OF TABLES

Table	Title	Page
1	EXPERIMENT SUMMARY . . . . .	13
2	COMPARISON OF EAGLE SERIES AND EDWARDS AFB SOURCE STRENGTH RESULTS . . . . .	31
3	COMPARISON OF EAGLE SERIES AND EDGEWOOD ARSENAL SOURCE STRENGTH RESULTS . . . . .	32
4	COMPARISON SUMMARY OF EAGLE TEST RESULTS, PREVIOUS TEST RESULTS, AND MODEL PREDICTION . . . . .	37
5	THE EAGLE 1 AND EAGLE 4 TEST CONDITIONS . . . . .	38
6	OXIDATION RATE OF NO IN AIR (AT STANDARD TEMPERATURE AND PRESSURE) . . . . .	42
7	COMPARISON OF OB/DG PREDICTIONS WITH THE EAGLE TEST RESULTS AT 785 METERS . . . . .	56
8	PLUME SPREADING PARAMETERS FOR OPEN-COUNTRY TERRAIN AND 100 METERS < x < 10 KILOMETERS . . . . .	58
9	RELATION BETWEEN WIND VARIABILITY ( $\sigma_\theta$ ) AND PASQUILL STABILITY CLASS . . . . .	60
10	COMPARISON SUMMARY OF THE EAGLE TEST RESULTS AND DISPERSION MODEL PREDICTIONS . . . . .	65

# LIST OF SYMBOLS

A	area
$C_p$	vapor cloud peak concentration (ppm)
$C_v$	volume fraction
$c_p$	specific heat at constant pressure
$H_v$	heat of vaporization
$M_s$	spill rate
$\dot{m}$	mass flow rate
p	pressure
Q	source strength
q	heat flux
R	gas constant for air
T	temperature
$T_*$	T-star, atmospheric temperature boundary layer parameter
t	time
$U_*$	U-star, atmospheric velocity boundary layer parameter
u	airspeed in x direction
w	source width in DDGD model
X	mass fraction
x	downwind coordinate
y	crosswind coordinate
z	vertical coordinate

## LIST OF SYMBOLS (CONCLUDED)

$\Delta$	difference or increment
$\sigma_{\theta, \phi}$	one standard deviation of the wind variability in the horizontal ( $\theta$ ) and vertical ( $\phi$ ) directions
$\sigma_{y, z}$	cloud spreading or dispersion parameter in the horizontal ( $y$ ) and vertical ( $z$ ) directions
$\omega$	absolute humidity

### subscript

A	air
c	evaporative cooling component
f	ground heat flux component
H <sub>2</sub> O	water vapor component
NO <sub>2</sub>	nitrogen dioxide component
s	source component
v	vapor component

## SECTION I

### INTRODUCTION

During the fall of 1983, the Lawrence Livermore National Laboratory (LLNL) conducted a series of large-scale (3-5 m<sup>3</sup>) nitrogen tetroxide (N<sub>2</sub>O<sub>4</sub>) spill tests for the U.S. Air Force Engineering and Services Laboratory, Tyndall AFB. The purpose of the test series was to determine the source strength characteristics and heavy-gas dispersion aspects of large N<sub>2</sub>O<sub>4</sub> spills. In addition, two spills were performed for the purpose of evaluating a Portable Foam Vapor Suppression System (PFVSS). The PFVSS tests were under the direction of the Ogden Air Logistics Center, Hill AFB, with support from USAF Space Division and the Strategic Air Command. The tests were performed at the U.S. Department of Energy (DOE) Nevada Test Site (NTS) under the jurisdiction of the DOE Nevada Operations Office (NVO).

The N<sub>2</sub>O<sub>4</sub> tests were the fifth in a continuing program of hazardous material spill tests conducted by LLNL and were code-named the Eagle series. Six N<sub>2</sub>O<sub>4</sub> spill tests were accomplished. Four tests were for the purpose of dispersion and source strength studies (Eagle 1, 2, 3, and 6) and two tests for evaluation of the PFVSS (Eagle 4 and 5). The Eagle series was conducted in conjunction with a series of four ammonia (NH<sub>3</sub>) spill tests (Desert Tortoise series) at considerable savings to both sponsors. These back-to-back series began with NH<sub>3</sub> on August 12, 1983, followed by the changeover to N<sub>2</sub>O<sub>4</sub> in mid-September. The Eagle series tests were performed between September 17 and October 30, 1983.

This report contains the analysis of the data obtained during the Eagle series spill tests as they pertain to the heavy-gas dispersion aspects of N<sub>2</sub>O<sub>4</sub> vapor clouds. As such, it deals primarily with the source strength and downwind dispersion results of the Eagle 3 and Eagle 6 spills. The final results of these spills are compared with concentration predictions of the Ocean Breeze/Dry Gulch (OB/DG) (Reference 1) and other simple dispersion models. The AFESC has suspected for some time (Reference 2) that the OB/DG model was inadequate for determining the hazardous corridor for accidental releases of N<sub>2</sub>O<sub>4</sub>. The primary purpose of this report is to quantify the discrepancy between the OB/DG predictions and the Eagle series results.

A complete description of the experiment and diagnostics for all six spill tests is contained in the Eagle Series Data Report (Reference 3), although a very brief description of the experiments is given in this report (Section II). The Data Report contains all of the data obtained during the test series. Those interested in the details of each experiment, or in additional data, are referred to Reference 3.

## SECTION II

### EXPERIMENT DESCRIPTION

#### A. FACILITY AND OPERATION

The two primary components of the temporary  $N_2O_4$  spill facility were an Air Force-supplied R-16 tanker and an LLNL high-pressure nitrogen ( $N_2$ ) gas tube trailer. A layout of the spill facility is shown in Figure 1. The  $N_2$  tube trailer was used to pressurize the R-16 tanker and force the  $N_2O_4$  through the spill pipe to the spill point, to provide purge gas for cleansing the piping system after each spill, and to provide gas pressure for the pneumatically operated valves.

A typical spill test sequence would proceed as follows. On days with favorable weather forecasts (proper windspeed and direction), the diagnostic system would be checked for satisfactory operation, and the spill area would be cleared of all personnel except for the arming team. Members of the arming team would open the manual valve on the  $N_2$  tube trailer, set the pressure control valve to the desired drive gas pressure and open the manual valves on the R-16 tanker. The arming team would then leave the area. All further spill operations were conducted by remote control.

When the windspeed and direction were within the designated acceptable spill conditions, the R-16 tanker was pressurized and the spill was initiated. A real-time display of the volume of  $N_2O_4$  spilled as a function of time was provided by the Command, Control Data Recording System (CCDRS) located about 1 kilometer upwind. When the desired amount of  $N_2O_4$  had been spilled, the spill was terminated. After the vapor cloud had cleared the downwind array, the pressure in the R-16 would be relieved and the disarming team would then enter the area and close the manual valves on the R-16 tanker to secure the facility.

The  $N_2O_4$  was delivered to the spill area by a 30-meter-long, 7.62-centimeter-diameter (3-inch) PVC pipe where it was distributed in two different ways as shown in Figure 2. The single-exit, confined spill configuration was for the purpose of studying evaporation rates as a function of liquid pool depth and windspeed. The multiexit, unconfined spill



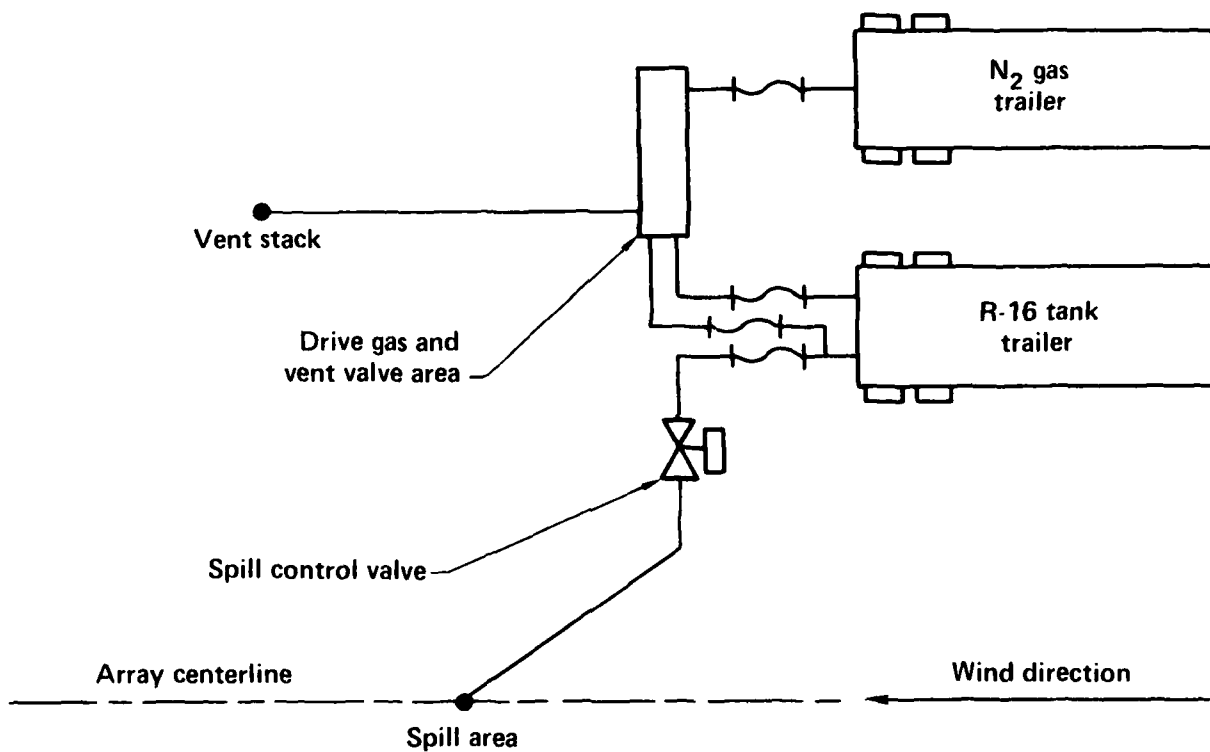
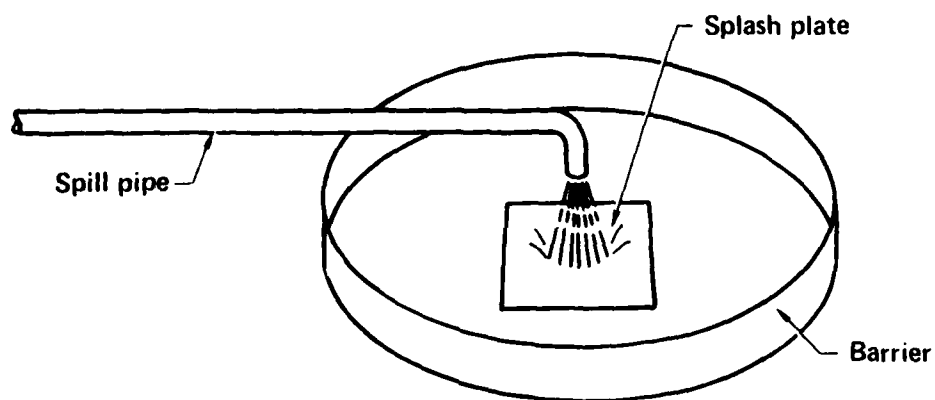
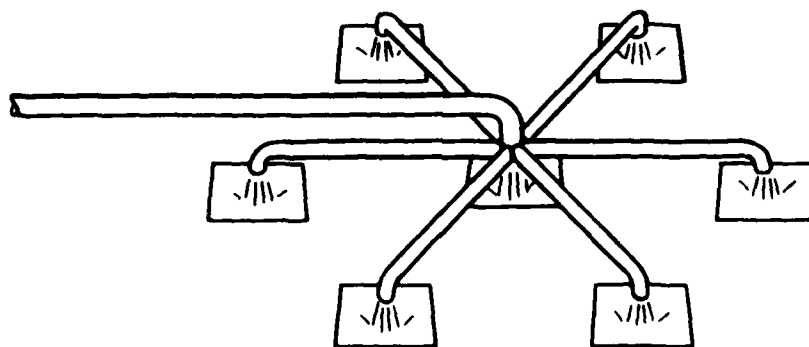


FIGURE 1. Eagle Series Spill Facility Site Layout



(a) Single-exit confined



(b) Multi exit unconfined

FIGURE 2. Eagle Series Spill Configurations

configuration was designed to distribute the  $N_2O_4$  over a large area so that it would evaporate as quickly as it was spilled. The intent was to produce a large well-defined source of  $N_2O_4$  vapor for the dispersion studies.

The Eagle 3 and Eagle 6 tests were unique because both involved spilling the remaining contents of the R-16 tankers. To insure that the R-16 was entirely empty, the nitrogen drive gas was allowed to blow through the R-16 and spill pipe system for several minutes after most of the liquid  $N_2O_4$  was exhausted. This acted as a purge, enhancing both the vaporization of the remaining liquid and the exhaust of this vapor from the entire system.

#### B. THE DIAGNOSTIC SYSTEM

Numerous measurements were made in the area of the spill. The temperature of the  $N_2O_4$  was recorded, just prior to its exit from the spill pipe. Three heat-flux sensors were placed just below the surface of the soil at different locations. A thermocouple rake assembly was also installed in the spill area to determine the temperature gradient within the liquid for the confined spills, and within the initial vapor layer of the unconfined spills. One thermocouple was at ground level, and the second and third were at heights of 2 and 4 centimeters, respectively. Provision was also made for measuring the depth (pressure head) of the liquid  $N_2O_4$  during the confined spills.

For tests Eagle 1 through 3 and Eagle 6, the  $N_2O_4$  was spilled directly onto the ground, whereas for Eagle 4 and 5 a PVC plastic liner was used to help contain the liquid. Although the playa surface of Frenchman Flat was clay-like and known for its impermeability to water, the  $N_2O_4$  soaked into it quite readily. In many cases it actually caused the surface to heave up several inches. There was considerable outgassing from the surface for several hours after the spill was terminated. After each of spills Eagle 1 thru 3 and Eagle 6, safety considerations required spraying 100-1000 gallons of water to dilute the  $N_2O_4$  absorbed by the ground to the point that its vapors were reduced to acceptable levels.

In addition to the spill area measurements, atmospheric boundary layer, wind field, vapor cloud temperature and concentration, and surface heat flux measurements were also made using an extensive diagnostic system developed by LLNL. There are three main array systems: the meteorological array, the mass flux array, and the dispersion array. The locations of these various arrays, along with the positions of the camera stations, are shown in Figure 3.

The meteorological array consisted of nine two-axis, cup-and-vane anemometers (all at a height of 2 meters), plus a 20-meter-tall tower located directly upwind of the spill area. The locations of the nine wind-field stations are shown in Figure 3. Windspeed and direction at each station were averaged for 10 seconds, and the results, plus the standard deviation of direction for the same 10-second period, were transmitted back to the CCDRS trailer. The wind-field data were displayed in real time and were the primary information used to determine the optimum time for the spill.

The meteorological boundary layer data were obtained from measurements mounted on a 20-meter tower located 50 meters directly upwind of the spill point (Figure 3). This tower was outfitted with four temperature gauges and three Gill bivane anemometers. This station also measured the ground heat flux. Humidity data and local barometric pressure were obtained from the NTS Weather Support Group.

A mass flux array was employed to determine the evaporation rate, or source strength, of the  $N_2O_4$ . This was to be accomplished by measuring the  $N_2O_4$  concentration, vapor cloud temperature and velocity as it passed through the array. Since  $N_2O_4$  dissociates quite rapidly to nitrogen dioxide ( $NO_2$ ), both species must be involved in the vapor flux. The  $N_2O_4/NO_2$  ratio would be determined using a well-documented equilibrium reaction rate constant. (References 4,5) The cloud temperature data are required both for calculations of the rate constant and the conversion from concentration to mass density. The product of the mass density and velocity integrated over the vapor cloud cross section yields the total mass flux passing through the array at any instant. If the entire cloud is "captured" by the array, this mass flux should be equivalent to the vapor source strength of the spilled  $N_2O_4$ .

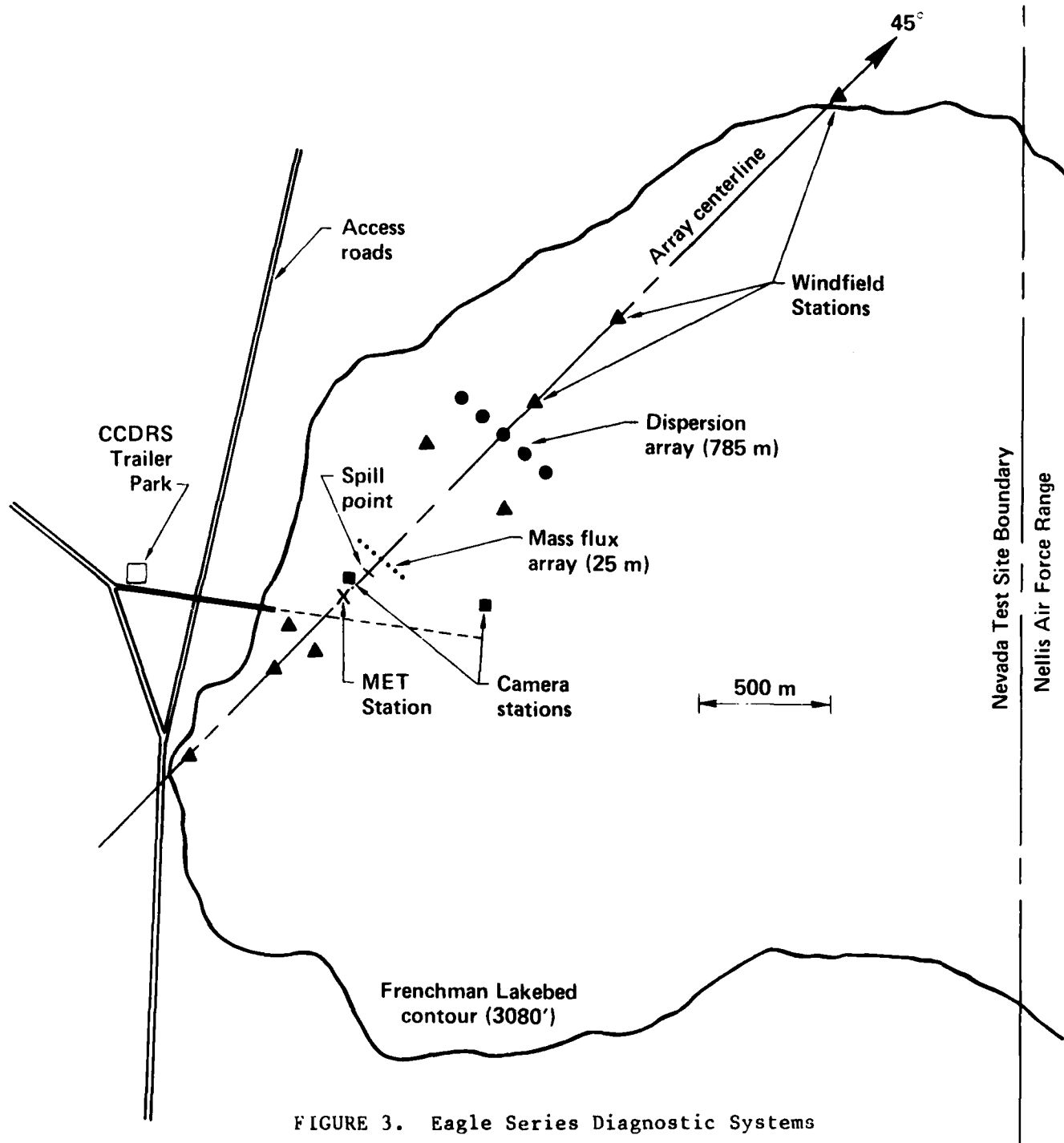


FIGURE 3. Eagle Series Diagnostic Systems

The mass flux array was located 25 meters downwind of the spill area and consisted of seven gas stations and two windspeed stations. The centerline station was a 10-meter-tall tower outfitted with three bivane anemometers, three LLNL infrared (IR) gas sensors, and three thermocouples. The three anemometers were located at heights of 1.3, 3, and 6 meters for the entire Eagle series. The IR gas sensors and thermocouples were located at different heights for each test. Six additional stations were located at 5-meter intervals to either side of the centerline station (three to each side). These stations had 6-meter-tall masts and each was outfitted with three LLNL IR gas sensors and three thermocouples.

A detailed description of the LLNL IR gas sensor is given in Reference 6. The sensor produces a signal proportional to the molecular absorption of IR radiation by the  $N_2O_4$  vapors as they pass through a 15-centimeter open-path sample region. The sensor was calibrated by using known concentrations of  $N_2O_4$ . The sensor was originally designed for the detection of liquefied natural gas (LNG) vapors and was not optimized for the Eagle series experiments to separately detect  $N_2O_4$  and  $NO_2$ . The species of most interest here was  $NO_2$ , however when it was discovered that the IR sensor was able to effectively detect  $N_2O_4$  vapors without any modifications, the cost savings dictated that this approach be taken. Unfortunately, measuring the  $N_2O_4$  concentration required placing the sensors very close to the source, which resulted in severe acid damage to several of them.

Two windspeed stations were located in the mass flux array at  $\pm 7.5$  meters to either side of the array centerline. These were similar to the wind-field stations described earlier, except that these anemometers were placed at a height of 1 meter above the ground. The purpose of these measurements was to determine if there were any windspeed variations as the vapor cloud passed through the array.

The dispersion array consisted of five 10-meter towers located 785 meters downwind of the spill area (see Figure 3). The purpose of this array of sensors was to record the extent of the vertical cross section of the  $NO_2$  vapors during each spill. All the towers had three  $NO_2$  gas sensors and three thermocouples located 1, 3.5, and 8.5 meters above the ground. The

towers were separated by a distance of 100 meters. The NO<sub>2</sub> gas sensors were manufactured by Energetic Sciences, Inc. (ESI) and were loaned to LLNL by the Shuttle Activation Task Force, Vandenburg AFB, for use during the Eagle series. All instruments were capable of full-scale measurements of 0-5, 0-50, and 0-500 ppm concentrations.

In addition to the gas sensors mounted on the towers of the 25 and 785 meters arrays, two portable NO<sub>2</sub> gas sensors were also used during the tests. These sensors used an electro-chemical transducer, and drew the gas sample through a short (approx. 0.5 meters) tube located about 15 centimeters above the ground. Both sensors had a maximum concentration range of 10 ppm NO<sub>2</sub>, and were refurbished and recalibrated by the manufacturer just prior to the Eagle test series. These sensors were used to obtain data at 2800 meters during the spill tests, and to monitor the CCDRS trailer park and the Frenchman Flat access roads overnight after the spills.

Photographic and video coverage of Eagle 1-3 were provided by LLNL. Photographic coverage of the PFVSS tests were the responsibility of Hill AFB. There was only video coverage of the Eagle 6 spill. The LLNL cameras were located as shown in Figure 3. Five cameras were used: two motion picture cameras and three programmable framing cameras. All cameras were remotely controlled and began operating when the spill valve was opened. The programmable cameras provided coverage for a total of 30 minutes at different framing rates. The motion picture coverage was for a duration of about 20 minutes. Black and white video coverage was provided by a TV camera located 20 meters directly upwind of the spill area. This camera was equipped with a remote zoom, pan and tilt capability, and was also used to monitor the facility arming and disarming procedure.

The control of the spills and the data acquisition and storage was all performed in the CCDRS trailer located at about 1 kilometer from the spill point (see Figure 3). This system utilizes UHF radio telemetry for command and data transmission and is designed to acquire data from sensors distributed over an area with a diameter of up to 10 miles (Reference 7). All of the remote data acquisition stations and sensors are battery-powered, portable,

gas-tight, and ruggedized. Batteries are recharged by solar cells. This network of 24 stations acquired data from up to 270 channels at a rate of one sample per second for the gas and control stations and one sample per 10 seconds for the windfield stations.

After each test, raw data are converted to fully calibrated data sets. These reduced data are written to an ASCII magnetic tape and transferred to the LLNL Computation Center for archival preservation. The data base tables are stored on an off-line mass storage system and are readily available for analysis.



### SECTION III

#### SOURCE STRENGTH RESULTS

It is imperative to dispersion model predictions that the source strength of the  $N_2O_4$  spill be known as accurately as possible. A preliminary analysis of the Eagle 3 spill test indicated that the OB/DG model tended to underpredict the  $NO_2$  concentrations at 785 meters downwind (Reference 8).

The underprediction varied from a factor of four to a factor of 300 due to the uncertainty in the preliminary source strength estimates. In this section, the source strength data will be analyzed in detail in order to reduce this range of uncertainty. The more accurate source strength estimates will then be used as input to several simple dispersion models to evaluate their prediction accuracy.

The source strength analysis that follows deals primarily with the Eagle 3 and Eagle 6 spills, although they were not designed specifically for the purpose of evaporation rate studies. This is because both spills produced good steady-state concentration data at 785 meters, a necessary requirement for validation of the simple dispersion models. For the purpose of comparison of the source strength and dispersion data with predictive models and/or other test results, a summary of the conditions of the Eagle 3 and Eagle 6 spills is given in Table 1. The average wind variability of Table 1 is the one-sigma value of the horizontal wind direction from station G01 at a height of 12 meters for the 1-hour period starting just before initiation of the spill. The  $\sigma_\theta$  values reported earlier (References 2 and 8) were for 3-minute time periods and were averages of all of the 2-meter-high wind-field stations. The  $\sigma_\theta$  values of Table 1 are from G01 so as to be consistent with the other atmospheric boundary layer parameters ( $R$ ,  $U_*$ ,  $T_*$ ), all of which were calculated from data obtained at this station.

The main reason for the uncertainty in the source strength of the Eagle spills has to do with the formation of a nitric acid ( $HNO_3$ ) mist and its impact on the 25-meter array concentration data. As outlined in Section II, the evaporation rate during each test was to be determined by measuring

TABLE 1. EXPERIMENT SUMMARY

Test:	Eagle 3	Eagle 6
Date	7 October 1983	30 October 1983
Time:	4:48 PDT	2:37 pm PST
Test Objective:	Dispersion data	Dispersion data
Spill Configuration:	Multiexit, unconfined	Multiexit, unconfined
Spill Volume:	4.2 m <sup>3</sup> (6090 kg)	3.4 m <sup>3</sup> (4930 kg)
Average Spill Rate:	1.4 m <sup>3</sup> /min (2030 kg/min)	0.7 m <sup>3</sup> /min (1015 kg/min)
Spill Duration:	180 sec	282 sec
N <sub>2</sub> O <sub>4</sub> Spill Temperature:	19°C	17.5°C
Prespill Ground Temperature:	27°C	28°C
Air Temperature @ 12 m:	21.9°C	22.6°C
Average Wind Speed @ 12 m:	3.66 m/sec	5.58 m/sec
Wind Variability @ 12 m:	$\sigma_\theta = 7.6^\circ$	$\sigma_\theta = 10.8^\circ$
Per Cent Cloud Cover:	95%	85%
Barometric Pressure:	907.9 mbars	909.3 mbars
Relative Humidity:	45%	35%
Richardson number (R) @12 m:	0.37	-1.216
U <sub>*</sub> :	0.081 m/sec	0.148 m/sec
T <sub>*</sub> :	0.189°C	-0.210°C

the vapor density and velocity as it passed through the 21 gas sensors located in a vertical plane 25 meters downwind of the spill area. The mass flux ( $\dot{m}$ ) at any instant in time is calculated by integrating the product of the vapor density and velocity over the entire cross section of the vapor cloud, i.e.,

$$\dot{m} = \int_A \rho_v u dA \quad (1)$$

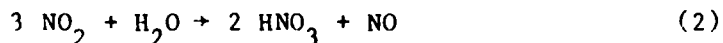
where  $\rho_v$  is the vapor density,  $u$  is the vapor velocity normal to the array plane, and  $A$  is the cloud cross-sectional area. The summation of the instantaneous mass flux ( $\dot{m}$ ) over the entire vaporization period should equal

the total amount spilled. This calculation of the total mass evaporation assumes no  $\text{N}_2\text{O}_4$  is lost due to permeation into the ground.

It became immediately obvious upon examination of the Eagle 1 spill results that something other than  $\text{N}_2\text{O}_4$  and/or  $\text{NO}_2$  vapors was present in the vapor cloud. The LLNL IR sensor detects molecular absorption in four different spectral regions. For mixtures of  $\text{N}_2\text{O}_4$  and  $\text{NO}_2$  vapors, two spectral regions would experience absorption (signal channels) while the other two would not (reference channels). If only  $\text{N}_2\text{O}_4$  or  $\text{NO}_2$  vapors were to pass through the sensor absorption region, one would expect to see strong attenuation in the signal channels and essentially none in the reference channels. For all of the Eagle series spills the observed attenuation in the reference channels was large.

Prior to the Eagle 3 spill, the IR sensors were tested using  $\text{N}_2\text{O}_4$  vapors directly from the R-16 tanker. The sensors behaved as expected, showing little attenuation in the reference channels. During the Eagle 3 spills, grab samples of the vapors were obtained as the cloud passed through the 25-meter array. A grab sample of the vapors from the  $\text{N}_2\text{O}_4$  in the spill pipe was also obtained. These grab samples were analyzed later at LLNL by both mass and IR spectroscopy. None of the grab sample results indicated the presence of a foreign gas capable of producing the broad-band (four-channel) attenuation observed in the Eagle series tests. It was concluded that the attenuation must be due to aerosol scattering which does produce broad-band attenuation. An  $\text{HNO}_3$  mist would also explain the severe acid damage which occurred to the instrumentation and structures in the 25-meter array during the spills. Furthermore, the photography of the spills showed a definite two-phase region within the vapor cloud. Consequently, it is believed that a  $\text{HNO}_3$  mist was formed in the earlier stages of the vapor cloud dispersion.

The source of the aerosol is believed to be a result of the gas-phase reaction of  $\text{NO}_2$  with the ambient humidity, i.e.,



This reaction, and the resulting  $\text{HNO}_3$  mist formation, have been studied in the past in regards to the scrubbing of  $\text{NO}_2$  gas from exhaust stacks (References 9-12). The reaction is extremely fast and experiments have shown that for typical atmospheric humidities and  $\text{NO}_2$  concentrations greater than 50 ppm, a  $\text{HNO}_3$  mist is instantly formed.

There are serious implications for the 25-meter array source strength estimates as a result of the  $\text{HNO}_3$  mist. It is well-known that the  $\text{N}_2\text{O}_4$  vapors dissociate quite rapidly to  $\text{NO}_2$  (References 4,5). The scavenging of the  $\text{NO}_2$  by the mist formation reaction will tend to increase the  $\text{N}_2\text{O}_4$  dissociation, hence reducing the  $\text{N}_2\text{O}_4$  concentrations at the 25-meter array. Furthermore, since the IR gas sensors were not calibrated for  $\text{HNO}_3$  mists, they can only produce estimates of the  $\text{N}_2\text{O}_4$  vapor content of the cloud. As a result, the  $\text{N}_2\text{O}_4$  concentrations presented in the Eagle Series Data Report (Reference 3) pertain only to the vapor portion of the cloud. The IR gas-sensor data was processed, assuming the mist attenuation to be equal in both the signal and reference channels.

A more accurate estimate of the Eagle 3 and 6 source strengths follows two different approaches. One approach estimates the evaporation rate using the spill area data, while the other involves a correction to the 25-meter vapor flux data. Each of these approaches will be discussed in the next two sections.

#### A. THE SPILL AREA HEAT SOURCE APPROACH

An estimate of the  $\text{N}_2\text{O}_4$  evaporation rate may be made by using the ground heat flux and vapor temperature data obtained in the area of the spill. The approach is to account for all of the heat sources to the  $\text{N}_2\text{O}_4$  during the spill, and using the heat of vaporization, calculate the vaporization rate. There are four main sources of heat for the  $\text{N}_2\text{O}_4$  as it is spilled onto the ground; ground heat flux, evaporative cooling (internal heat), solar insolation, and heat from the air. Only two of these four (ground heat flux and evaporative cooling) were measured during each spill test. Because of the overcast skies and the strong absorption of the sun's radiation by the  $\text{N}_2\text{O}_4$  vapor, solar insolation was probably not a strong heat source for either Eagle

3 or 6. However, the heating by the air could have been significant. Thus, the source strength determined from the ground heat flux and evaporative cooling data alone will be an underestimate of the actual evaporation rate.

The source strength ( $\dot{m}_s$ ), as determined from the available spill area heat source data, may be thought of as consisting of the sum of two components

$$\dot{m}_s = \dot{m}_f + \dot{m}_c \quad (3)$$

where  $\dot{m}_f$  is the evaporation associated with heat flux from the ground and  $\dot{m}_c$  is the evaporation associated with the heat loss due to evaporative cooling of the liquid  $N_2O_4$ . The ground heat flux component is given by

$$\dot{m}_f = \frac{qA}{H_v} \quad (4)$$

where  $q$  is the measured heat flux averaged over the spill area  $A$ , and  $H_v$  is the heat of vaporization (414 Joules/gm). The evaporative cooling component is given by

$$\dot{m}_c = \frac{M_s c_p \Delta T}{H_v} \quad (5)$$

where  $M_s$  is the spill rate,  $c_p$  is the specific heat of the liquid  $N_2O_4$  and  $\Delta T$  is the temperature difference between the  $N_2O_4$  at the spill pipe exit and the  $N_2O_4$  vapors immediately above the ground surface. The second component of the source strength ( $\dot{m}_c$ ) assumes that the  $N_2O_4$  liquid on the ground and its pure vapor at a height of 2 centimeters are at the same temperature, and that evaporation occurs at the expense of the spilled liquid's internal energy.

Estimates of the source strength of both the Eagle 3 and 6 spills have been made, using the spill area heat source approach of Equation (3).

#### 1. The Eagle 3 Test

The ground heat flux during the Eagle 3 spill was recorded at three locations approximately 1 meter from one of the multiexit spill ports. The average of the heat flux at these three locations is shown in Figure 4a, where a negative flux indicates heat flow out of the ground. The temperature difference between the  $N_2O_4$  in the spill pipe and the vapor just above the

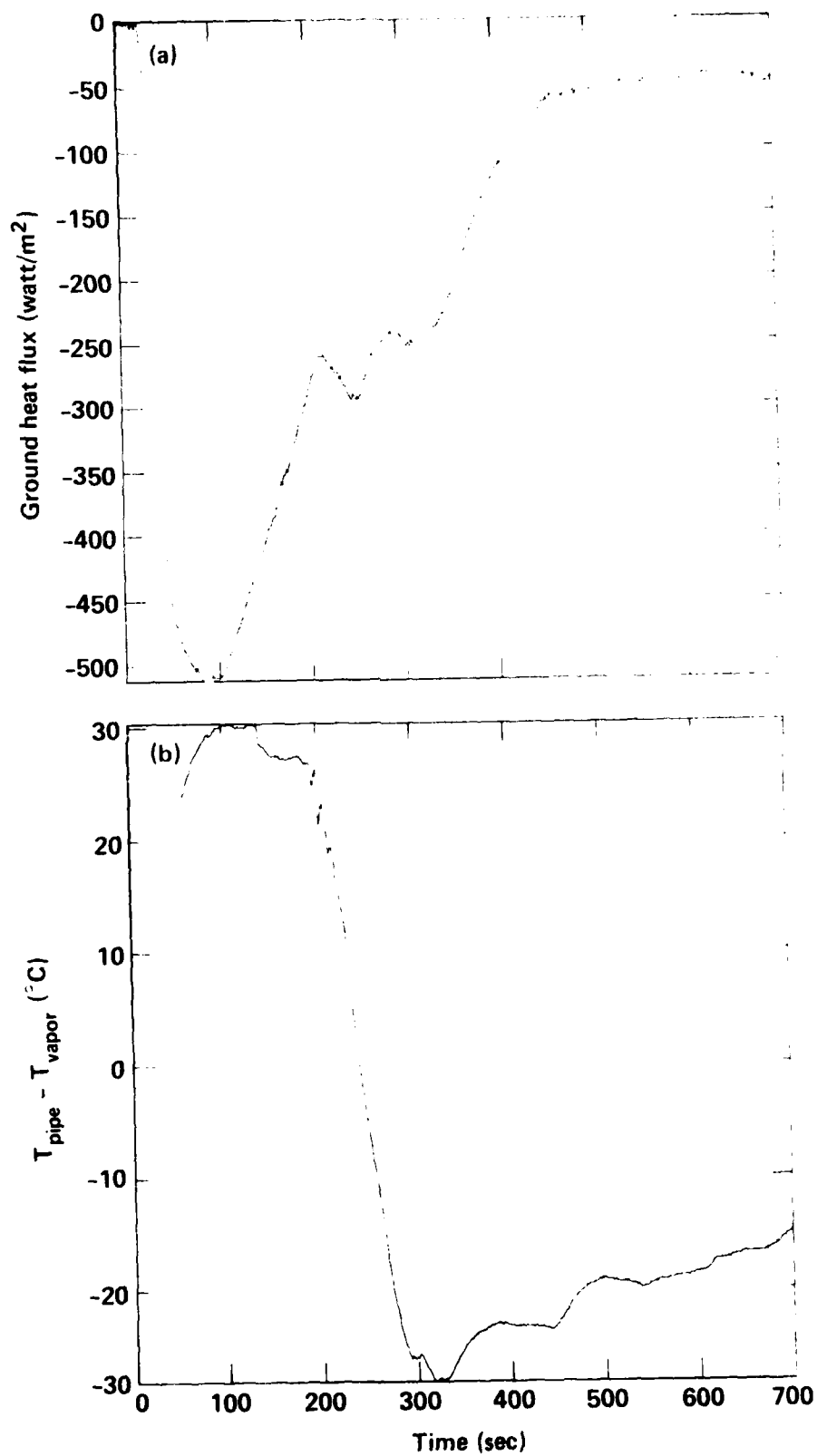


FIGURE 4. Eagle 3 Spill Area Heat Source Data

ground surface is given in Figure 4b. The data of Figure 4a are used in Equation (4) for  $Q$ , and the data of Figure 4b is the  $\Delta T$  of Equation (5).

The Eagle 3 spill consisted of all the  $N_2O_4$  remaining in the R-16 tanker ( $4.2 \text{ m}^3$ ). Consequently, the spill was not terminated by closing the spill valve. The  $N_2$  drive gas was allowed to flow through the R-16 and the spill pipe for about 2 minutes to completely purge the system of all  $N_2O_4$  liquid and/or vapor. This produced an "artificial" increase in the source strength, since the  $N_2O_4$  vapor was now coming from both the surface and the spill pipe. This also produced a colder temperature in the spill pipe than was recorded near the ground (negative  $\Delta T$  in Figure 4b). The elimination of the liquid from the R-16 was indicated by an abrupt drop in the tanker pressure, which occurred at  $t = 188$  seconds. Taking into account the initial delay in the valve opening, the true source strength of the Eagle 3 spill is believed to be in effect only for about 180 seconds.

The evaporative cooling ( $m_c$ ) and ground heat flux ( $m_f$ ) components of the Eagle 3 source strength are shown in Figures 5a and 5b. As can be seen, the evaporative cooling produces a much larger contribution to the evaporation rate than does the ground heat flux component. This is a result of the large liquid surface area to volume ratio created by the multiexit spill apparatus. The internal heat capacity of the thin layer of liquid  $N_2O_4$  is not large enough to supply the energy necessary to satisfy the heat of vaporization requirements. As a result, the  $N_2O_4$  undergoes a large drop in temperature to supply the required energy. For spills which are allowed to pool, this may not be the case. For instance, the Eagle 4 and 5 spills which confined the liquid and allowed it to pool to depths of 3-5 centimeters did not produce vapor temperatures as cold as those of the Eagle 3 spill.

The spill area used in the calculation of the ground heat flux component (Figure 5a) was taken to be  $314 \text{ m}^2$ , which is equivalent to a mean diameter of 20 meters. The presence of the  $N_2O_4$  on the desert soil was quite obvious, and appeared to include all of the surface within the dimensions of the multiexit spill configuration. The edges of the spill area were not that of a perfect circle, however, the 20-meter-diameter estimate is felt to be realistic.

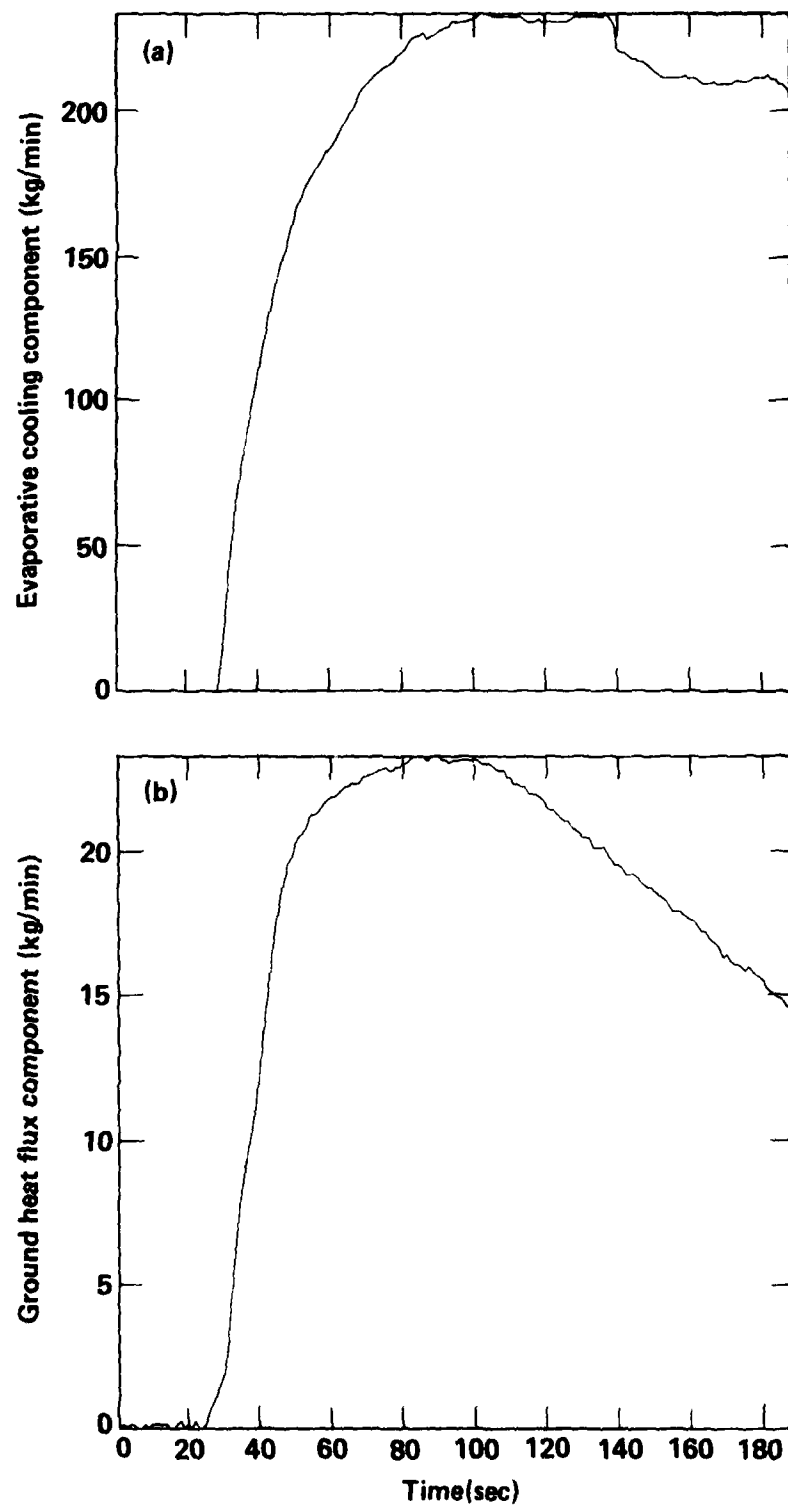


FIGURE 5. Eagle 3 Spill Area Source Strength Components



The total source strength of the Eagle 3 spill is shown in Figure 6. These results do not include contributions from insolation or heating from the air, and as such must be viewed as conservative estimates of the Eagle 3 source strength.

## 2. The Eagle 6 Test

The Eagle 6 spill (like the Eagle 3 spill) consisted of the remaining  $N_2O_4$  in the R-16 tanker, with the last of the liquid being followed by a  $N_2$  purge of the system. This purge began at  $t = 296$  seconds which includes an initial delay of about 14 seconds, hence, the realistic duration of the Eagle 6 spill is only about 282 seconds.

The liquid  $N_2O_4$ , ground and air temperatures for the Eagle 6 spill were essentially the same as those for the Eagle 3 spill, but the Eagle 6 spill was at about half the spill rate of the Eagle 3 spill. The Eagle 6 test was the last of the series and was conducted after the PFVSS tests. As a result, the ground surface conditions were no longer level, and some of the spill area diagnostics were inoperable or of questionable accuracy by this time. Two ground heat flux sensors were located near the center of the multiexit spill apparatus, but due to the surface roughness, only one of them appeared to give reasonable results. There also were problems with the vapor temperature measurements. Two thermocouples were located in the vicinity of the heat flux sensors, but the recorded temperatures were considerably warmer than for the Eagle 3 spill. This may also have been a result of the surface roughness, making the actual measurement height above the liquid surface much greater than expected and/or allowing for local pooling of the liquid.

All of the factors just mentioned cast considerable doubt on the Eagle 6 source strength estimates based on the spill area data. The two components resulting from this approach are shown in Figure 7, and the total Eagle 3 source strength is shown in Figure 8. The results of Figure 8 are believed to greatly underestimate the Eagle 6 source strength, but are presented here for completeness.

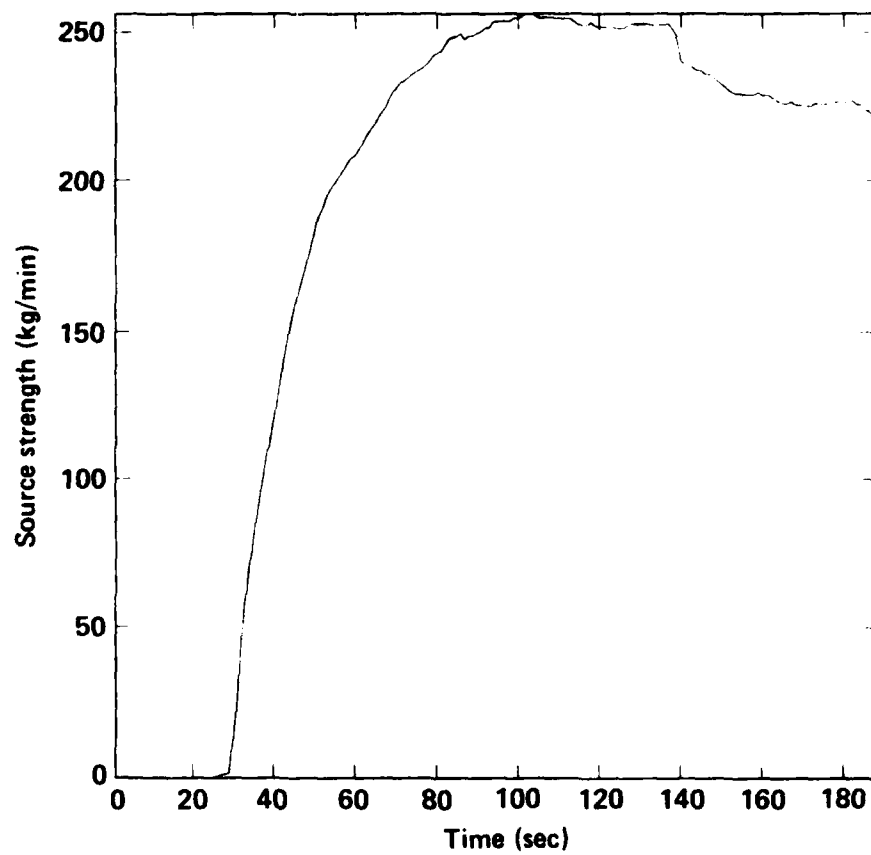


FIGURE 6. Eagle 3 Source Strength Estimate Using the Spill Area Heat Source Approach

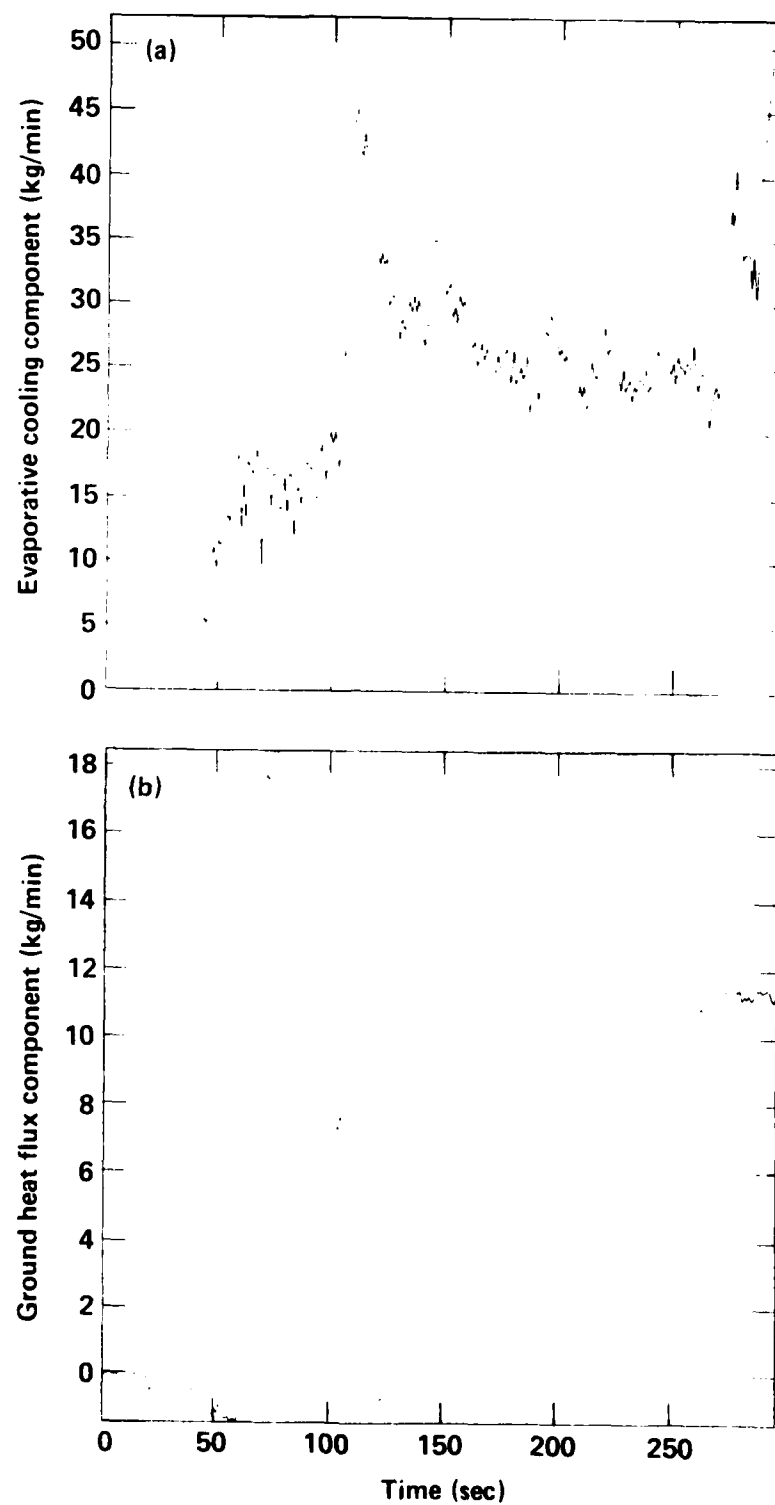


FIGURE 7. Eagle 6 Spill Area Source Strength Components

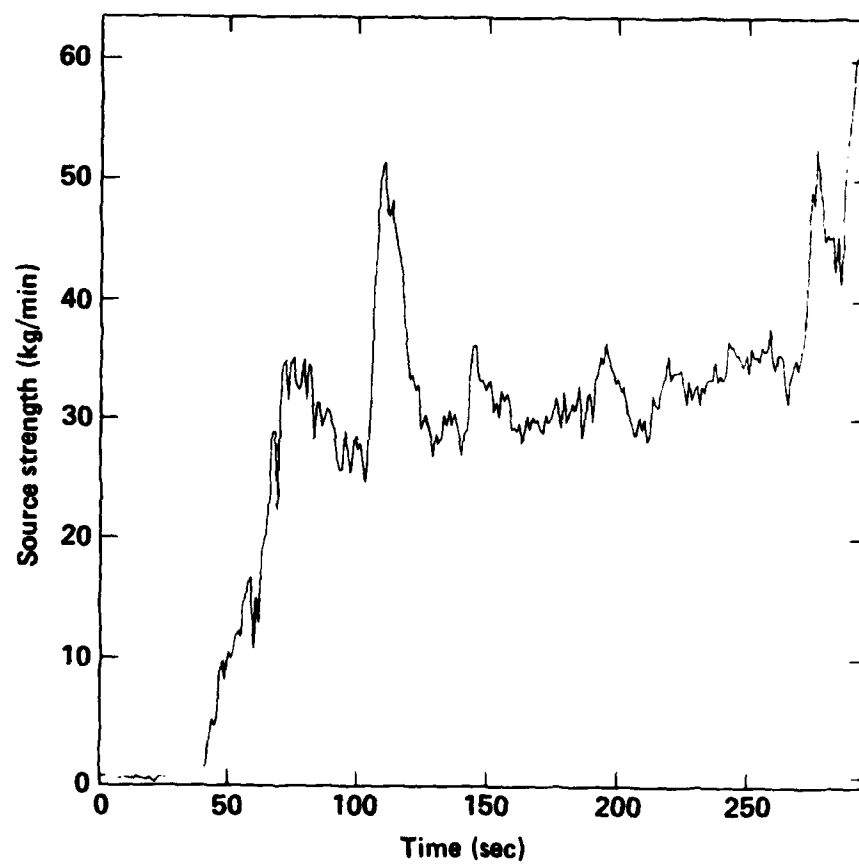


FIGURE 8. Eagle 6 Source Strength Estimate Using the Spill Area Heat Source Approach

It is clear that the  $N_2O_4$  did not evaporate as quickly as spilled for either Eagle 3 or Eagle 6; consequently, the source strength should not be totally dependent on the spill rate. Considering the other similarities between the two spills, one would expect the Eagle 3 and Eagle 6 evaporation rates to be very similar.

#### B. THE MIST FORMATION APPROACH

The mist formation approach involves an estimate of the amount of the  $N_2O_4$  vapor which is converted to  $HNO_3$ , which is then added to the measured vapor flux. Both the instantaneous vapor flux and the cumulative vapor mass total passing through the 25-meter array for the Eagle 3 and Eagle 6 spills are shown in Figure 9. As mentioned in Section II, this result considers only the  $N_2O_4$  and  $NO_2$  gas component of the vapor cloud--it does not include the  $HNO_3$  mist contribution. The vapor flux calculation of Figure 9 assumes a linear interpolation between the concentration values recorded at each sensor location. To account for the vapor below the lower level of sensors, extrapolations of the data were required. Two techniques were used to extrapolate the vertical concentration data to the ground level. If the concentration at the middle height of a station was less than the lower height value, the ground level concentration was determined by using a quadratic curve through these two values whose slope (concentration gradient) is zero at the ground. For cases where the middle height concentration was greater than the lower height value, the ground level concentration was determined by a linear extrapolation of these two values.

For the Eagle 3 spill, the width of the  $N_2O_4$  vapor cloud was greater than the width of the 25-meter array ( $\pm 15$  m). To account for the vapors passing outside the array in the mass flux calculation, two artificial stations were set at  $\pm 20$  meters, each with zero gas concentration at all three heights. The vapor distribution was assumed to vary linearly between the actual  $\pm 15$ -meter station data and the artificial (zero)  $\pm 20$ -meter stations. These corrections were not required for the Eagle 6 spill.

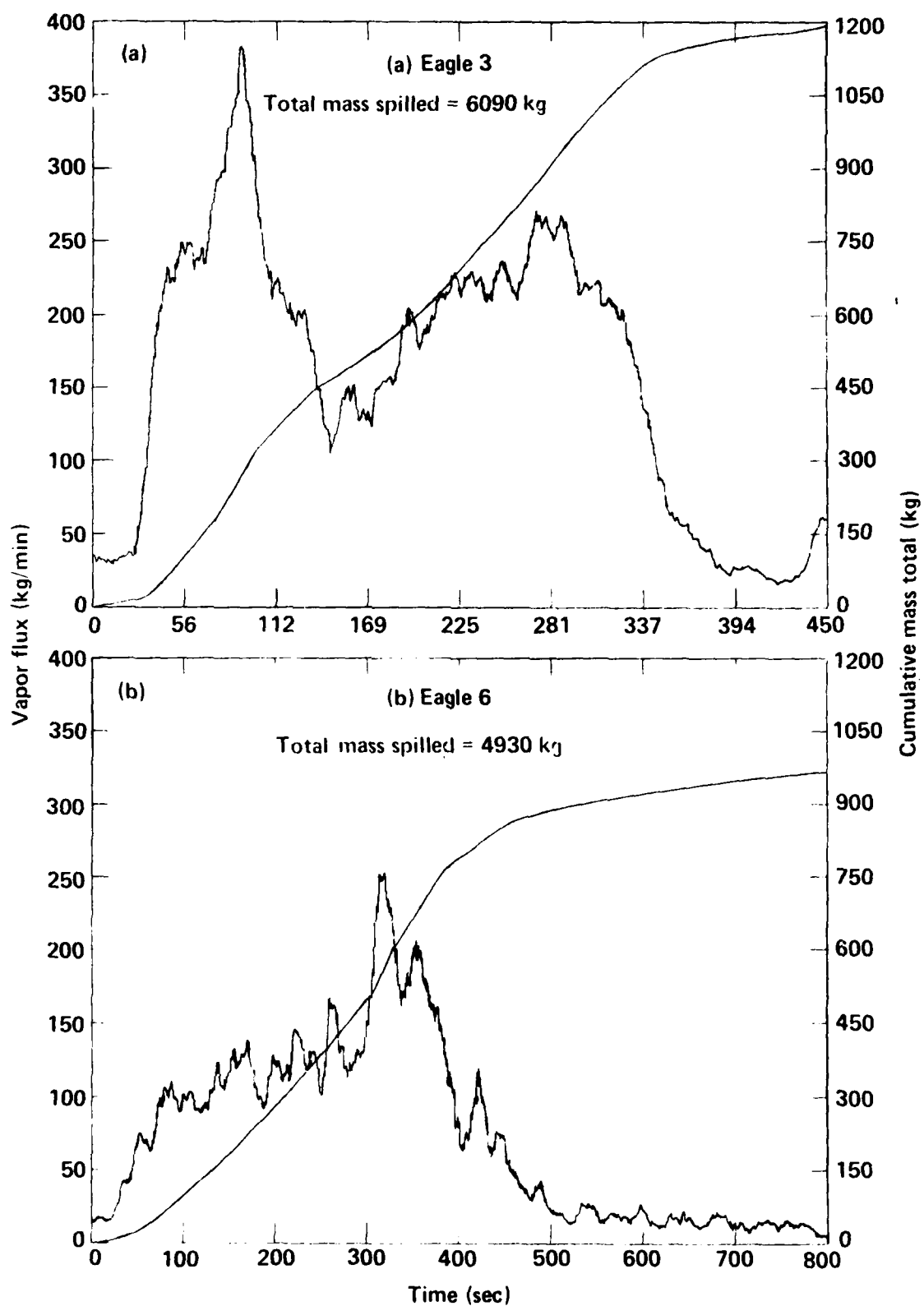


FIGURE 9.  $\text{N}_2\text{O}_4$  and  $\text{NO}_2$  Vapor Flux at 25 meters for the Eagle 3 and Eagle 6 Spills

As indicated in Figure 9, there is a large discrepancy between the cumulative mass total and the total mass spilled in each case, 6090 and 4930 kilograms, respectively. This discrepancy is a result of both the absence of the  $\text{HNO}_3$  mist contribution during this time period and the delayed release of the vapor due to the permeation of the  $\text{N}_2\text{O}_4$  into the soil.

We can calculate the source strength of the Eagle 3 and Eagle 6 spills if we can estimate the mass flux of the  $\text{HNO}_3$  mist and add this to the vapor flux-data of Figure 9. It is known that the  $\text{HNO}_3$  mist is primarily a result of the reaction of the  $\text{NO}_2$  and the ambient humidity. If we assume that all of the ambient water vapor reacts to form  $\text{HNO}_3$ , then we can calculate the mass fraction of the  $\text{HNO}_3$ .

We begin the mist formation approach by looking at the species composition of the  $\text{N}_2\text{O}_4$  vapors prior to any  $\text{H}_2\text{O}$  and  $\text{NO}_2$  reaction. The mass fractions of the cloud components are given by

$$X_A + X_{\text{H}_2\text{O}} + X_S = 1 \quad (6)$$

where  $X_A$  is the dry air mass fraction,  $X_{\text{H}_2\text{O}}$  represents the humidity mass fraction and  $X_S$  is the total mass fraction of the  $\text{N}_2\text{O}_4$  and  $\text{NO}_2$  vapors. If we let  $X_{\text{NO}_2}$  represent that mass fraction of  $\text{NO}_2$  that reacts with the  $\text{H}_2\text{O}$  to form  $\text{HNO}_3$ , we can then rewrite Equation (6) as

$$X_A + X_{\text{H}_2\text{O}} + X_{\text{NO}_2} + X_V = 1 \quad (7)$$

where  $X_V$  is the mass fraction of the  $\text{NO}_2$  and  $\text{N}_2\text{O}_4$  vapor which would pass through the 25-meter array and produce the results of Figure 9. Conversely, the sum  $X_{\text{H}_2\text{O}} + X_{\text{NO}_2}$  is that fraction of the mixture which forms the  $\text{HNO}_3$  mist. However, a mass balance of the chemical reaction of Equation (2) tells us that the  $\text{NO}_2$  and  $\text{H}_2\text{O}$  react in a ratio of 7.67 to 1, or

$$X_{\text{NO}_2} = 7.67 X_{\text{H}_2\text{O}} \quad (8)$$

if all of the  $\text{H}_2\text{O}$  is converted to  $\text{HNO}_3$  and  $\text{NO}$ . We also know that

$$X_{\text{H}_2\text{O}} = \omega X_A \quad (9)$$

where  $\omega$  is the absolute humidity of the ambient air at the time of the spill. Combining Equations (7)-(9), we get

$$X_A + X_{H_2O} + 7.67 \omega X_A + X_V = 1$$

and if we compare this result with Equation (6) we see that

$$X_S = X_V + 7.67 \omega X_A \quad (10)$$

Neglecting the small volume change of the air/vapor mixture when the mist forms, one may express the mass fraction as a density fraction, and Equation (10) may be expressed as

$$\rho_S = \rho_V + 7.67 \omega \rho_A \quad (11)$$

where  $\rho$  is now the mass density of each of the species (S,V,A). We can further reduce Equation (11) to measurable quantities by use of the ideal gas law, i.e.,

$$\rho_S = \rho_V + \frac{7.67 \omega p_A}{RT_A} \quad (12)$$

where  $R$  is the gas constant for air, and  $p_A$  and  $T_A$  are its partial pressure and temperature. If we assume that the vapor and mist are in thermal equilibrium, and that the partial pressure of the air is equal to the total pressure of the vapor/mist mixture, then we may correct the data of Figure 9 by the additional density term in Equation (12) in the mass flux calculation of Equation (1). The values used for  $p_A$  and  $T_A$  were the site barometric pressure and the temperature data of the 25-meter array.

The results of the mist formation correction to the vapor flux data for the Eagle 3 and Eagle 6 spills are shown in Figure 10. As can be seen, the mist correction essentially doubles the vapor flux results of Figure 9. The mist contribution to the results of Figure 10 should be a slight overprediction since the  $NO_2 + H_2O$  reaction may not have reached 100 percent completion and the air partial pressure will always be less than the total pressure. However, the  $HNO_3$  mist formation is quite rapid (References 9-12) and the assumption of 100 percent completion is probably accurate. And



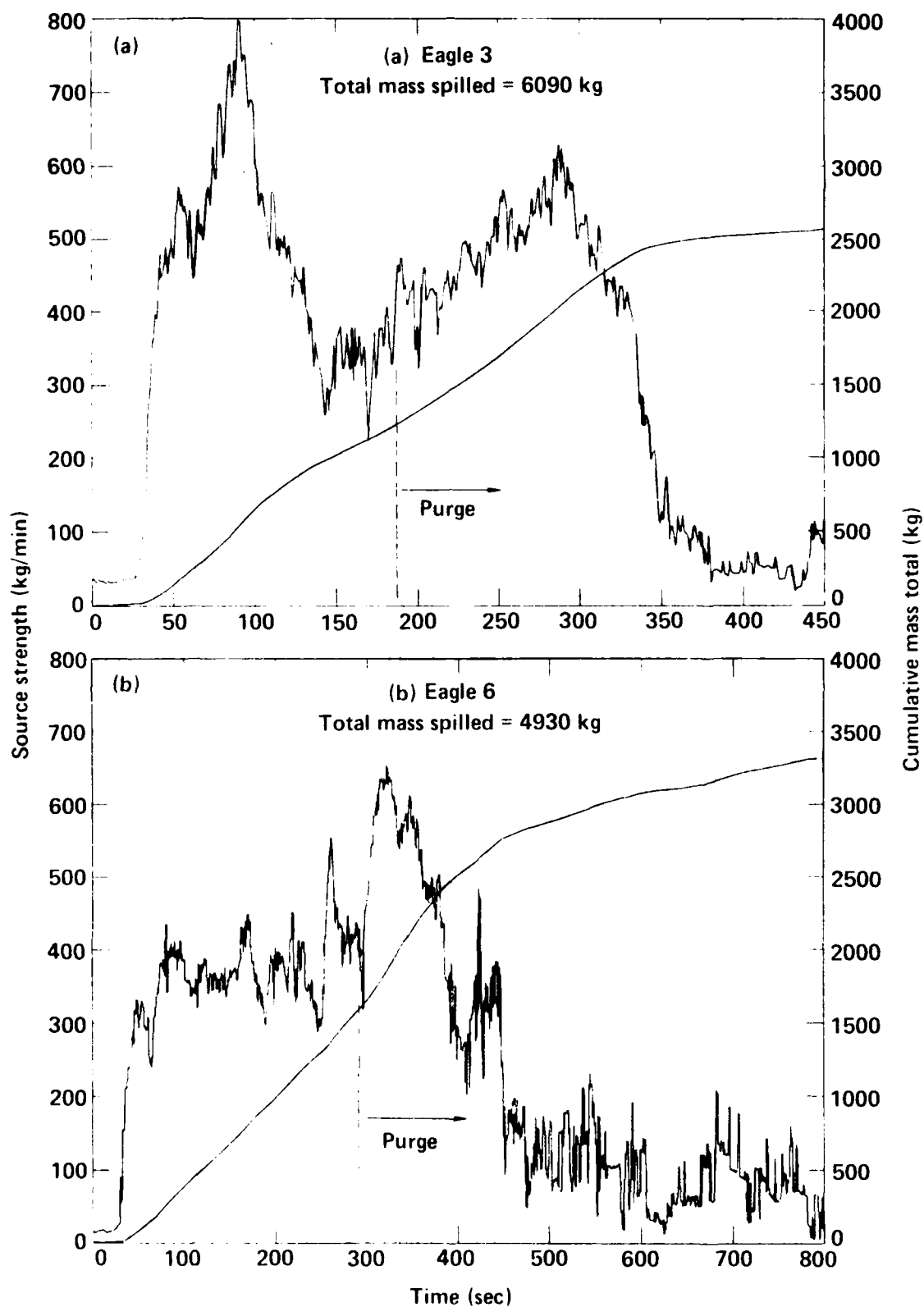


FIGURE 10. Eagle 3 and Eagle 6 Source Strength Estimates Using the Mist Formation Approach

since the  $\text{N}_2\text{O}_4$  and  $\text{NO}_2$  concentrations at the 25-meter array were seldom greater than 1 percent by volume, the use of the total pressure (barometric) instead of the air partial pressure should result in only a minor error.

It would not be appropriate to use the mist formation approach for source strength estimates after the initiation of the  $\text{N}_2$  gas purge of the spill system. The purging introduced large amounts of dry  $\text{N}_2$  into the region of the spill area, making the humidity during these time periods less than that in effect prior to the purge. Without accurately knowing the absolute humidity ( $\omega$ ), the mist component correction to the measured vapor density (Equation 12) can not be performed.

It is also evident from Figure 10 that only about half of the total mass spilled evaporated during the first 7 or 8 minutes of the test. Outgassing from the surface was observed to continue for hours after the spill was terminated. In fact, the spill area had to be soaked with water after the Eagle 3 and Eagle 6 tests in order to reduce the vapors to safe levels for entry the following day.

#### C. THE EAGLE 3 and EAGLE 6 SOURCE STRENGTHS

The source strengths of the Eagle 3 and Eagle 6 spills have been calculated by two approaches. The results of Figure 6 and Figure 8 use the spill area data and are believed to underestimate the source strength, especially for the case of Eagle 6. The results of Figure 10 use the 25-meter vapor flux measurements with a correction for the mass of the  $\text{HNO}_3$  mist, and are believed to slightly overestimate the source strengths in both cases. It is felt that the source strengths calculated by the mist formation approach are more accurate. Since these calculations are known to slightly overestimate the evaporation rates, 90 percent of the values of Figure 10 will be used as the Eagles 3 and 6 source strengths. As mentioned previously, these source strengths are felt to be accurate only up to the beginning of the  $\text{N}_2$  purge.

There is a further consideration to be addressed concerning the results of Figure 10. In the remainder of this report, the Eagle 3 and Eagle 6 source strengths will be compared to data of previous experiments, to source strength model predictions, and will be used as input for comparison of the

downwind concentration data with some simple dispersion model predictions. In practically every case, the comparison will require a steady-state value for the source strength data. As shown in Figure 10, the Eagle 3 and Eagle 6 evaporation rates were not steady, and some method of determining an effective value must be arrived at for use in these steady-state comparisons. As mentioned in Section III A, the relevant source strengths of both spills are in effect only for those times up to initiation of the  $N_2$  purge. This corresponds to times less than 180 seconds for Eagle 3, and less than 282 seconds for Eagle 6 as are indicated on Figure 10. The effective steady-state source strength for the Eagle 3 and Eagle 6 spills is taken to be 90 percent of the average source strength of Figure 10 for the relevant spill durations of 180 and 282 seconds, respectively. This results in effective steady-state source strengths of 410 kilograms/minute for Eagle 3, and 344 kilograms/minute for Eagle 6. These effective steady-state values will be used in the comparisons that follow.

#### D. SOURCE STRENGTH DATA OF PREVIOUS TESTS

Two major  $N_2O_4$  source strength tests were performed prior to the Eagle test series. The first was conducted in 1962 at Edwards AFB by Space Technology Laboratories, Inc., (Reference 13) and the second was completed in 1965 at the U.S. Army Edgewood Arsenal (Reference 14). These tests will be briefly described, and the appropriate results compared to the Eagle 3 and Eagle 6 source strength estimate of the previous section.

##### 1. The Edwards AFB Tests

The Edwards AFB source strength tests were a follow-on to the OB/DG dispersion model development program (Reference 1). The goals of the test program were to determine the evaporation rates of  $N_2O_4$  under conditions applicable to typical TITAN II launch installations. This was accomplished by using the data from numerous small tests (5-10 kilograms) to produce an empirical model of the evaporation rate vs. windspeed, propellant temperature, spill area, and mass. This empirical formula was then validated by a series of larger tests (900 kilograms). The tests included not only spills on ground, concrete, and water, but also spills from various heights as may occur

in a missile silo. The rates were generally very high initially, then slowly decreasing as a result of evaporative cooling of the  $N_2O_4$ . In many cases the  $N_2O_4$  surface was observed to freeze-over. There is no discussion in the report (Reference 13) as to how these evaporation rates were measured.

The results of the Edwards AFB tests were compiled into a series of working curves which express the source strength as a function of windspeed, spill area, and propellant temperature. The ground temperature was not considered in these experiments. The spill scenario closest to that of the Eagle tests was one involving  $N_2O_4$  spills on dry concrete. Although these curves were actually generated using the maximum evaporation rate for each test, they are presented as representing steady-state source strengths. For the Eagle 3 and Eagle 6 test conditions, the curves give estimated source strengths for spills on concrete of 942 and 1212 kilograms/minute, respectively. However, the report states that the source strength should be reduced by a factor of from 3 to 5 for spills on soil. This reduction is due to seepage of the liquid  $N_2O_4$  into the soil. The Edwards AFB results are compared with the Eagle series estimated source strength data in Table 2. The Edwards AFB source strengths of Table 2 are those from the spills on concrete reduced by a seepage factor of four.

TABLE 2. COMPARISON OF EAGLE SERIES AND EDWARDS AFB SOURCE STRENGTH RESULTS  
(kilograms/minute)

<u>Test</u>	<u>Edwards AFB Predictions</u>	<u>Eagle Series Results</u>
EAGLE 3	236	410
EAGLE 6	303	344

We see that the Edwards AFB and Eagle series source strength results compare quite nicely. However, there is the question as to why the Edwards AFB predicted Eagle 3 rate is less than the Eagle 6 rate. This is believed to be due to the strong dependence of the Edwards AFB results on the windspeed. The propellant temperature effect is much smaller, and tends to actually increase the Eagle 3 source strength. The strong windspeed dependence of the Edwards AFB data probably has to do with the small size of the spills. These

small vapor sources are easily affected by windspeed and atmospheric turbulence, whereas the larger Eagle series spills produce sources which tend to create their own environment. The larger spills actually buffer the liquid surface from the ambient wind conditions, and as a result are not as greatly affected by air speed and temperature as are the smaller spills.

## 2. The Edgewood Arsenal Tests

A series of  $N_2O_4$  source strength tests were performed at the U.S. Army Edgewood Arsenal under the sponsorship of the U.S. Air Force. There were a total of 17 tests over a 16-month period beginning in 1963. Each test consisted of about 45 kilograms ( $0.03 \text{ m}^3$ ) of  $N_2O_4$  which was spilled into a square (4 ft by 4 ft) pan suspended from a load cell. Source strength data were obtained for several different pan bottom substrates, including concrete and beach sand. The diagnostics included measurements of the  $N_2O_4$ , air, and substrate temperatures prior to and during the evaporation process, as well as the ambient atmospheric conditions.

There was no attempt to consolidate the Edgewood test data for empirical correlations of the various test parameters. Consequently, we can only choose the particular test that most closely represents the Eagle 3 and Eagle 6 spills. The closest substrate material was dry beach sand, and although there were three spills with this material, only two produced believable results. One of these tests was done during extremely cold weather ( $1^\circ\text{C}$ ) and with high windspeeds ( $11.6 \text{ m/sec}$ ), putting it well away from either of the Eagle 3 or Eagle 6 spill conditions (see Table 1). The conditions of the other test (Edgewood 10), as well as the source strength results, are compared to the Eagle source strength estimates in Table 3.

TABLE 3. COMPARISON OF THE EDGEWOOD ARSENAL AND EAGLE SERIES SOURCE STRENGTH RESULTS

Test	$N_2O_4$ Temperature ( $^\circ\text{C}$ )	Sand Temperature ( $^\circ\text{C}$ )	Air Temperature ( $^\circ\text{C}$ )	Wind Speed ( $\text{m/sec}$ )	Source Strength ( $\text{kg/min}$ )
Edgewood 10	4.4	15	11	2.2	135
Eagle 3	19	27	21.9	3.66	410
Eagle 6	17.5	28	22.6	5.58	344

We see from Table 3 that the Edgewood source strength of Test 10 was considerably less than for the Eagle 3 and Eagle 6 spills. However, the similarity between the tests is minimal. The Edgewood test was performed at much colder ambient temperatures and a lower windspeed, both of which would tend to reduce the evaporation rate.

The Edgewood results are typically less than the Edwards source strengths, which are less than the Eagle series estimates. Perhaps there is a hint here of a spill size, or scaling effect, since the Edgewood tests at 45 kilograms were less than the largest Edwards tests of 900 kilograms, which were smaller yet than the Eagle spills of 6090 and 4930 kilograms. This spill size scaling effect on the  $N_2O_4$  source strength would require a more in depth analysis into the similarities (or differences) between the various spill test conditions before any sound conclusions may be drawn. This effort is beyond the scope of this analysis report.

#### E. COMPARISON OF EAGLE RESULTS WITH SOURCE STRENGTH MODEL PREDICTIONS.

To complete the Eagle series source strength data analysis, the Eagle 3 and Eagle 6 source strength estimates will be compared with those predicted by currently used evaporation rate models. In this section heavy use is made of the work of Kunkel (Reference 15), who just recently compared several source strength models for various hydrazine and  $N_2O_4$  spill scenarios. The predictive accuracies of the Ille and Springer (I&S) model (Reference 16), the Shell evaporation model (Reference 17), the Army model (Reference 18), the Air Force Engineering and Services Laboratory (ESL) model (Reference 19), and the Air Weather Service (AWS) model (Reference 20) will be evaluated. None of these four models deal with the  $N_2O_4$  spill rate or seepage into the soil. In all but the Shell evaporation model, it is assumed that the liquid material is instantaneously released onto the entire spill area, equilibrium is established immediately, and the evaporation rate is constant for all time. The Shell evaporation model does allow for the temporal variations of the source strength after an instantaneous spill into a known area. In the comparisons that follow, a spill area of  $314 \text{ m}^2$  was used in all cases. No effort is made to describe these models in any great detail, only those aspects of each model which are in direct contrast with the Eagle series spill conditions are mentioned. Those requiring further information about these models are directed to the respective References 15-19.

For the readers convenience, a table containing a summary of the source strength results is provided at the end of this section.

### 1. The Ille and Springer Model

The I&S (Reference 16) model was one of the more sophisticated source strength models evaluated by Kunkel (Reference 15) in that it includes insolation, evaporative cooling, heating by the air, liquid pool depth, and both windspeed and turbulence effects. The model assumes that the initial  $N_2O_4$  temperature is the same as the air temperature, but the liquid is allowed to cool as it satisfies a set of energy balance requirements including radiative and convective heat transfer. However, the cooling of the liquid to its equilibrium value is assumed to occur quickly, and this heat loss is not converted to mass loss in the final source strength result. As discussed in Section III A, the evaporative cooling is a major contribution to the Eagle series source strength.

A version of the I&S model, revised to include  $N_2O_4$  spills, was exercised for the Eagle 3 and Eagle 6 spill conditions by Captain Larry Key (Tyndall AFB). The spill input criteria assumed a pool depth of 5 mm and an "n factor," or wind stability constant, of 0.182. The insolation was set to closely match the ground heat flux recorded at the upwind meteorological station. The results of these model predictions for the Eagle 3 and Eagle 6 spill conditions were 183 and 243 kilograms/minute, respectively. The source strengths predicted by the I&S model are less than the estimated Eagle 3 and Eagle 6 values (410 and 344 kilograms/minute, respectively), and show the same strong dependence on the windspeed as do the Edwards AFB and Edgewood Arsenal data. The predicted  $N_2O_4$  pool temperatures for Eagle 3 and Eagle 6 were  $-13^{\circ}C$  and  $-14.6^{\circ}C$ , respectively, showing excellent agreement with the recorded vapor temperatures directly above the spill area.

### 2. The Shell Evaporation Model

The Shell evaporation model used in this report is the source strength portion of the SPILLS evaporation and air dispersion model (Reference 17) developed by the Shell Development Co., Houston, Texas. The model predicts source strength as a function of time for several spill scenarios. It accounts for heat transfer from the ground and the air, but neglects radiative heating

from the sun. While the model calculates the source strength contribution of the flashing of liquefied gases down to atmospheric pressure, it assumes the resulting liquid pool to remain at its normal boiling point until it is completely evaporated. There is no provision for evaporative cooling of the liquid or the source strength contribution resulting from this process. The Shell evaporation model was programmed and exercised for the Eagle 3 and Eagle 6 spill conditions by Bruce Kunkel (AFGL). The necessary input parameters were supplied by Radian, Corp., who use the Shell evaporation model for the source strength portion of a hazardous response code developed under the sponsorship of Tyndall AFB.

The spill scenario most applicable to the Eagle spills was that of the instantaneously formed pool, which for the initial  $N_2O_4$  conditions produced no flash contribution to the source strength. This resulted in average source strength predictions of 191 kilograms/minute for Eagle 3 and 284 kilograms/minute for Eagle 6. Both of these predictions are less than the estimated source strengths for Eagle 3 (410 kilograms/minute) and Eagle 6 (344 kilograms/minute), and reflect a strong windspeed dependence. The Shell evaporation model results are quite close to the I&S model results even though the liquid pool temperatures are quite different ( $-13^{\circ}\text{C}$  and  $-14.6^{\circ}\text{C}$  for I&S,  $21.9^{\circ}\text{C}$  and  $22.6^{\circ}\text{C}$  for Shell).

### 3. The Army Model

The Army source strength model was adapted from the Chemical Engineers Handbook (Reference 21), and depends on the windspeed, spill area, air temperature, and the liquid molecular weight, density, and vapor pressure. This model does not account for heat transfer due to radiation or evaporative cooling, and assumes the pool temperature to remain constant and equal to the ambient air value. The results of the Army Model for the Eagle 3 and Eagle 6 spill conditions are 299 and 431 kilograms/minute, respectively. With this model, the source strength variation between these two predictions is totally a function of the windspeed ( $u^{0.8}$ ). These predicted source strengths are about twice as large as those produced by the I&S model. This is not too surprising since the Army model holds the  $N_2O_4$  temperature, and as a result its vapor pressure, at much higher values than the I&S model and the Eagle spill conditions.



#### 4. The ESL Model

The ESL model (Reference 19) is a simplification of the I&S model which requires only the windspeed, spill area, a pool temperature factor, and a material volatility factor. The pool temperature factor allows for a reduction in the source strength as the liquid pool evaporatively cools, while the volatility factor takes into account the effect of pool temperature on the  $N_2O_4$  vapor pressure. The ESL model is very sensitive to the choice of pool temperature, consequently, it was exercised for both the recorded vapor temperature ( $-10^\circ\text{C}$ ) and the ambient air temperature ( $22^\circ\text{C}$ ).

The ESL model predictions for the Eagle 3 spill conditions are 327 kilograms/minute for a pool temperature of  $-10^\circ\text{C}$ , and 682 kilograms/minute for a pool temperature of  $22^\circ\text{C}$ . The ESL model results for the Eagle 6 spill conditions are 461 kilograms/minute for a pool temperature of  $-10^\circ\text{C}$ , and 960 kilograms/minute for a pool temperature of  $22^\circ\text{C}$ . The predicted source strength for Eagle 6 is considerably larger than the estimated result (344 kilograms/minute), once again showing a strong windspeed dependence ( $u^{0.75}$ ).

#### 5. The Air Weather Service Model

The AWS model (Reference 20) is the simplest of all, depending only on the windspeed, spill area, and the  $N_2O_4$  vapor pressure at  $26^\circ\text{C}$ . The model is an empirical one, derived from laboratory-scale experiments.

The AWS model predicts a source strength of 244 kilograms/minute for Eagle 3, and 352 kilograms/minute for the Eagle 6 windspeed. The correlation is not bad, considering the simplicity of the model. In this model, the source strength is also strongly proportional to the windspeed ( $u^{0.8}$ ), which results in the larger prediction for Eagle 6 than for Eagle 3.

#### F. SUMMARY AND DISCUSSION OF SOURCE STRENGTH RESULTS

A comparison of the Eagle 3 and Eagle 6 source strength estimates with the results of previous tests and source strength model predictions is summarized in Table 4. In general, the previous test results and model predictions are within about a factor of 2 of the Eagle source strength estimates.

TABLE 4. COMPARISON SUMMARY OF EAGLE TEST RESULTS, PREVIOUS  
TEST RESULTS AND MODEL PREDICTIONS

	<u>Source Strength</u> (kg/min)	
	<u>Eagle 3</u>	<u>Eagle 6</u>
Eagle Test Results	410	344
Edwards AFB Spill Tests	236	303
Edgewood Arsenal Spill Tests	135	135
I&S Model	183	243
Shell Evaporation Model	191	284
Army Model	299	431
ESL Model (-10°C pool temperature)	327	461
ESL Model (+22°C pool temperature)	682	960
AWS Model	244	352

#### 1. Experimental Comparisons

We will first discuss the source strength differences between the Eagle results and the Edgewood and Edwards results. It is the opinion of the author that these source strength differences are a direct result of the size differences of the spill tests; i.e., a scaling phenomenon. The small size of the Edgewood and Edwards tests resulted in a strong windspeed dependence, plus a great deal of scatter in the results of seemingly identical experiments (Reference 19). The small releases of these previous experiments (< 900 kilograms) created vapor sources which were easily penetrated by the wind. Because of the small amount of vapor mass relative to the local air mass, the air was able to mix with and remove the vapor from the liquid surface at maximum efficiency. This produced the strong windspeed dependence and the freezing/thawing of the liquid surface that occurred during both sets of experiments. For the larger Eagle tests in which the  $N_2O_4$  was allowed to pool (EAG 4, EAG 5), there was some subcooling of the liquid, but the surface did not freeze. Furthermore, if windspeed truly dominates the evaporation rate, then the Eagle 3 source strength should be less than that of the Eagle 6 spill, and it is not. Large-scale releases, such as the Eagle spills, produce evaporation sources so intense that the atmospheric boundary layer is actually perturbed. These effects have actually been measured during large liquefied natural gas spills (Reference 24). The intense generation of these vapors to some degree buffers the liquid surface from the local ambient environment. Future source strength experiments must be of adequate size to reproduce these effects; otherwise, they will produce erroneous results.

Another apparent discrepancy between the Eagle tests and the Edgewood/Edwards tests has to do with the effect of the  $N_2O_4$  seepage into the soil. Both the Edgewood and Edwards tests indicate that ground seepage results in a reduction in source strength relative to evaporation from similar spills on solid surfaces such as concrete or metal. This does not appear to be the case for the Eagle tests, at least not for the confined spills. Both the Eagle 1 and Eagle 4 tests were confined spills conducted under very similar conditions as shown in Table 5. However, the Eagle 1 spill was done directly onto the soil whereas the Eagle 4 spill was done on several layers of a thin (10 mil) plastic liner, thus, eliminating the effect of ground seepage without appreciably changing the heat flux from the ground. As we see from Table 5, the Eagle 1 spill produced six times larger  $N_2O_4$  vapor concentrations at 25 meters than did the Eagle 4 spill. This would seem to indicate in this case that ground seepage may have actually increased the source strength rather than decreasing it. Differences in the other experiment parameters; such as, spill rate, pool depth and air temperature must also be taken into account here, but it would appear that for the Eagle tests, ground seepage produced quite different results than for the Edwards and Edgewood tests.

TABLE 5. THE EAGLE 1 AND EAGLE 4 TEST CONDITIONS

	<u>Spill Rate</u> <u>(m<sup>3</sup>/min)</u>	<u>Spill</u> <u>Volume</u> <u>(m<sup>3</sup>)</u>	<u>N<sub>2</sub>O<sub>4</sub></u> <u>Temperature</u> <u>(°C)</u>	<u>Air</u> <u>Temperature</u> <u>(°C)</u>	<u>Wind</u> <u>Speed</u> <u>(m/sec)</u>	<u>N<sub>2</sub>O<sub>4</sub></u> <u>@ 25 m</u> <u>(% vol)</u>
EAG 1	1.75	1.3	19.0	34.0	6.15	0.4
EAG 4	0.5	2.8	19.8	24.5	4.94	0.07

The depth of the liquid pool also appears to be an important factor in determining the  $N_2O_4$  source strength. In both the Edwards and Edgewood tests the  $N_2O_4$  liquid surface was reported to freeze and thaw several times throughout the evaporation period. All of these previous experiments involved pool depths less than 2 centimeters. As explained earlier, the unconfined Eagle 3 and Eagle 6 spills, which allowed very little liquid pooling at all, also resulted in near-freezing source temperatures. However, the Eagle 4 and Eagle 5 spills produced pool depths of 4 and 9 centimeters, respectively, but no surface freezing was observed in either case. There was

some cooling of the liquid during both experiments with a minimum pool temperature of  $-3^{\circ}\text{C}$  occurring during the Eagle 5 test. This pool depth effect on the source strength may be explained in the following manner. As the  $\text{N}_2\text{O}_4$  vapors are carried away from the source, evaporation from its surface must occur in order to satisfy the liquid surface vapor pressure requirements. This evaporation requires heat, which the liquid must obtain from its own internal energy (specific heat) if the supply from external sources is inadequate. If the pool depth is large, then so is the available mass of  $\text{N}_2\text{O}_4$  per unit surface area, and the required temperature drop of the liquid will be small. However, as the mass per unit area of the liquid becomes small, the temperature drop must increase until, finally, the liquid reaches its freezing point. Consequently, when comparing source strengths of confined spills, one must pay particular attention to the depth of the liquid pool.

Finally, in regard to the comparison of the small and large-scale experiments, there is the matter of the spill rate. For the small-scale spills, the spill was almost instantaneous and not very important when comparing one spill test with another. However, for spill volumes on the order of the Eagle series, the spill rate is important since the spill duration for these large volumes is long (3 to 5 minutes), and in the case of the unconfined tests (Eagle 3 and 6), essentially corresponds to the duration of the maximum source strength. This was the case even though it was clear that the liquid did not evaporate as quickly as it was spilled. In this respect, the small-scale and large-scale tests are difficult to compare. It would seem that many accidental releases of  $\text{N}_2\text{O}_4$  would not be instantaneous, and for these cases the spill rate may be an important parameter in determining the magnitude of the source strength.

## 2. Model Comparisons

Many of the source strength phenomena discussed in the previous paragraphs also apply to comparisons of the Eagle results with the source strength model predictions. This is because the AWS model was derived from curve fits to source strength experimental data, and the I&S, Shell evaporation, Army, and ESL models were most likely influenced by the same results. For example,

all models predict a strong dependence on the windspeed--a conclusion one would draw upon examination of the small-scale test results. All but the I&S model neglect the evaporative cooling of the liquid, and yet, according to the Eagle 3 data, this mechanism accounts for about half of the source strength. The I&S model does include the pool depth, although a parameter sensitivity analysis by Kunkel (Reference 15) shows the model to be relatively insensitive to this parameter. The results of the Eagle series tests indicate that pool depth is an important factor. Finally, none of the models deal with the spill rate or ground seepage effects, both certainly being realistic scenarios for an accidental release. However, at this time it is not clear how spill rate or ground seepage affects the source strength of large spills.

It is surprising, perhaps even fortuitous, that the source strength model predictions and the Eagle test results correlate as well as they do. Many of the parameters used in the predictions of Table 4 (vapor pressure, pool temperature, windspeed effect) differ by large factors from the measured values, yet the predicted results are within a factor of two of the measured source strengths. Whereas there certainly appears to be room for source strength model improvement in regard to  $N_2O_4$  spills, it is doubtful that the Eagle test series produced enough data to construct an improved empirical model. The evaporation of  $N_2O_4$  when spilled on soil or concrete is a very complicated process and will depend strongly on the spill scenario (spill rate, substrate material, confinement, etc.). The most economical approach would be to improve and/or develop a sophisticated analytical source strength model which contains all of the important physics, and compare this new model with Eagle and other test results or future large-scale source strength experiments. This sophisticated model could then possibly be used to assist in the development of less complex source strength models.

## SECTION IV

### VAPOR CLOUD DISPERSION RESULTS

The primary objective of this section is the comparison of the downwind NO<sub>2</sub> concentration data with the OB/DG and several other simple dispersion models. Whereas there are many sophisticated heavy-gas dispersion models available (most requiring large mainframe computers); the Air Force is at present considering upgrading its predictive capability only for models which are useable with currently available personal computer systems. The comparisons of these simple models will deal with only the downwind concentration data of the Eagle 3 and Eagle 6 tests and will use the source strength results of Table 4, and the atmospheric conditions of Table 1. The dispersion models examined in this section include the OB/DG model (Reference 1), the steadystate Gaussian Plume model (Reference 25), the Shell Dispersion model (Reference 17), and the CHARM model (Reference 26). However, prior to the description and comparison of these model predictions with the data, we will first analyze the downwind NO<sub>2</sub> data as to its quality since this is crucial to the analysis.

#### A. NO<sub>2</sub> DOWNWIND DATA ANALYSIS

The goal of the following analysis is the determination of the appropriate vapor cloud concentration levels at 785 meters for comparison with dispersion model predictions. In order to completely describe the vapor cloud at 785 meters downwind, concentration measurements of the decomposition and reaction products HNO<sub>3</sub>, NO, and NO<sub>2</sub> must be known since each of these species makes up a significant portion of the initial vapors (Equation 2). Unfortunately, the magnitude of the mist formation was not anticipated, and the ESI gas sensors in the 785-meter array were responsive only to NO<sub>2</sub>. In the case of the NO content of the vapor cloud, it is believed that this component oxidizes to NO<sub>2</sub> according to



This reaction depends on the  $O_2$  concentration and the square of the NO concentration. The oxidation times necessary for half the NO present in air at various initial concentrations to be completely oxidized to  $NO_2$  are given in Table 6. As can be seen, significant amounts of NO could still be expected at 785 meters, since the cloud transit time to this downwind location was about 4 minutes for Eagle 3, and 2.5 minutes for Eagle 6.

TABLE 6. OXIDATION RATE OF NO IN AIR (AT STANDARD TEMPERATURE AND PRESSURE)

<u>NO (ppm)</u>	<u>half-life (minutes)</u>
20,000 (2%)	0.175
10,000 (1%)	0.35
1,000	3.5
100	35.0

The situation concerning the eventual fate of the  $HNO_3$  mist is not clear at all. The vapor pressure of pure  $HNO_3$  at  $20^\circ C$  is about 50 Torr, while that of a 50 percent mixture with water is only 0.355 Torr (Reference 21). However, Goyer (Reference 9) found that at relative humidities less than 20 percent, the  $HNO_3$  mist evaporated quite rapidly. So there is the question as to how much of the  $HNO_3$  mist evaporates, and then what fraction of the  $HNO_3$  vapor decomposes to  $NO_2$ . The latter process was studied by England and Corcoran (Reference 10) and Johnston, et al. (Reference 23) with the general conclusions that the decomposition at ordinary temperatures is rather slow (second-order) unless NO is present, then the reaction becomes first order. Consequently, there is reason to suspect that a significant portion of the vapor from the source may have passed through the 785-meter array in some form other than  $NO_2$ . In this respect, the vapor cloud concentration data (expressed in this report as  $NO_2$  in ppm) must be considered as minimum levels. Had all of the  $N_2O_4$  vapor decomposed completely to  $NO_2$  vapor, the  $NO_2$  concentration levels at 785 meters would have been much larger. A conservation of mass calculation using a Gaussian cross-section representation of the cloud dimensions at 785 meters is used to estimate the maximum  $NO_2$  levels.

## 1. The Eagle 3 Test

We next address the timing of the choice of  $\text{NO}_2$  concentration level at the 785 meter array so that it coincides with the prepurge source strength estimate of Section III A. We must also consider the effect of the cloud meander on these results. A superposition of the  $\text{NO}_2$  concentration results at 785 meters for the Eagle 3 spill is given in Figure 11. These data are all at a height of 1 meter, with the G22 station on the array centerline, G23 to the left and G21 to the right as one looks downwind (see Figure 3). As we see from Figure 11, the cloud arrived initially at the left side of the array (G23), then slowly moved across the centerline (G22) to the right side (G21). Unfortunately, the appropriate source strength period, as discussed in Section III A, is only 180 seconds, and during this time period, according to the data of Figure 11, essentially all of the  $\text{NO}_2$  vapor was recorded by only one station, G23. The large ( $> 500$  ppm)  $\text{NO}_2$  concentrations recorded by stations G22 and G21 for  $t > 500$  seconds were a result of the nitrogen purge of the R-16 tanker which was exhausted out the spill pipe. Stations G20 and G24 saw no measurable  $\text{NO}_2$  concentrations.

The decrease in the  $\text{NO}_2$  concentrations at G23 (Figure 11) between 300 and 400 seconds is believed to be due to the meander of the vapor cloud centerline away from station G23. This meander makes accurate determination of the peak cloud concentration levels difficult. We see that G22 also recorded a small concentration level ( $\sim 10$  ppm) just prior to  $t = 300$  seconds, which would seem to indicate that the cloud centerline was between G23 and G22 at this time. It would have been desirable to have had more gas-sensor stations separated by less than 100 meters. However, only 13  $\text{NO}_2$  sensors could be borrowed in time for these experiments, and the station spacing was a compromise with the  $\text{NH}_3$  test requirements to keep both experiments within budget.

The location of the Eagle 3 cloud centerline between stations G22 and G23 is also somewhat substantiated by cloud centerline trajectory estimates constructed from the 9 wind-field stations (Figure 3). Windspeeds, direction, and  $\sigma_\theta$  data from these nine stations were interpolated and extrapolated to a 200-meter wide by 2800-meter-long grid beginning at the spill point and



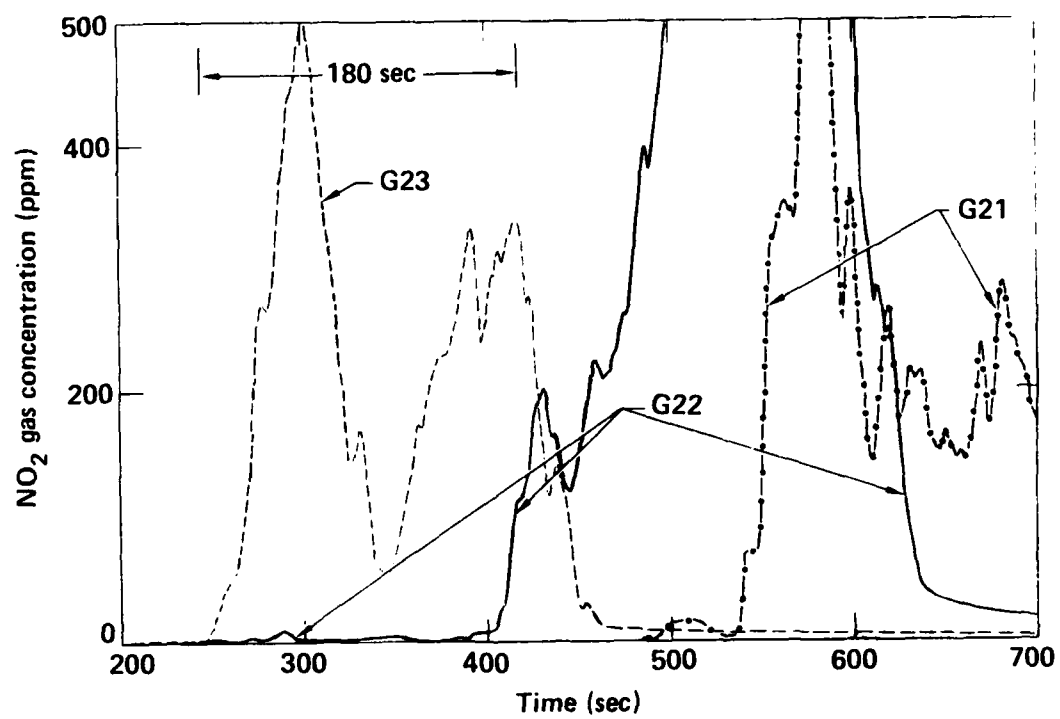


FIGURE 11. The Eagle 3 NO<sub>2</sub> Concentration Data (1 meter high, 785 meters downwind)

straddling the array centerline. These data were then used to track hypothetical particles released every 10 seconds during the spill. The results for selected times during the Eagle 3 test are shown in Figure 12. The centerline of cloud travel is indicated in each plot by a solid line. Using the interpolated  $0_{\theta}$  data, trajectories were also constructed for hypothetical particles tracked along wind directions of the centerline trajectory  $\pm 0_{\theta}$ . These ever-widening trajectories, indicated by dotted lines, display the lateral dispersion of these hypothermal particles associated with a spreading rate equal to the measured wind-field fluctuations. These trajectories are determined by only a few stations within the area included in Figure 12, hence the centerline location is not precise. In fact, the trajectories of Figure 12 do not show the cloud passing over stations G23 or G21, yet the data of Figure 11 do show it contacted these locations. However, the trajectories do substantiate the conclusions that most of the vapor cloud was generally between stations G22 and G23.

Two problems concerning the  $\text{NO}_2$  data at 785 meters (Figure 11) have been discussed; the missing NO and  $\text{HNO}_3$  vapor concentrations, and the effect of the cloud meander from one station to another. Both of these phenomena would tend to make the concentration levels at 785 meters larger than those actually displayed in Figure 11, but the extent of this discrepancy is not known. For the purpose of the model data comparisons to follow, the minimum Eagle 3 cloud centerline concentrations will be taken as those which were measured at  $t = 300$  seconds (500 ppm). The crosswind concentration distribution at  $t = 300$  seconds for the Eagle 3 test are shown in Figure 13. The reader is further cautioned that the width and symmetrical shape of the cloud in Figure 13 is somewhat misleading. These contours are the result of a linear interpolation of the data from the three levels of station G23 only; stations G22 and G24 observed no gas at this particular time. It is actually believed that the cloud centerline is slightly to the right of the +100 location of Figure 13, and the overall cloud width is probably less than 200 meters.

In the model/data comparisons to follow, both the concentrations and the cross-sectional size of the model predictions will be compared to the data of Figure 13. Since all of the models involved in this analysis assume a crosswind Gaussian concentration distribution, it will be helpful in comparing cloud heights and widths to have an equivalent Gaussian representation of the

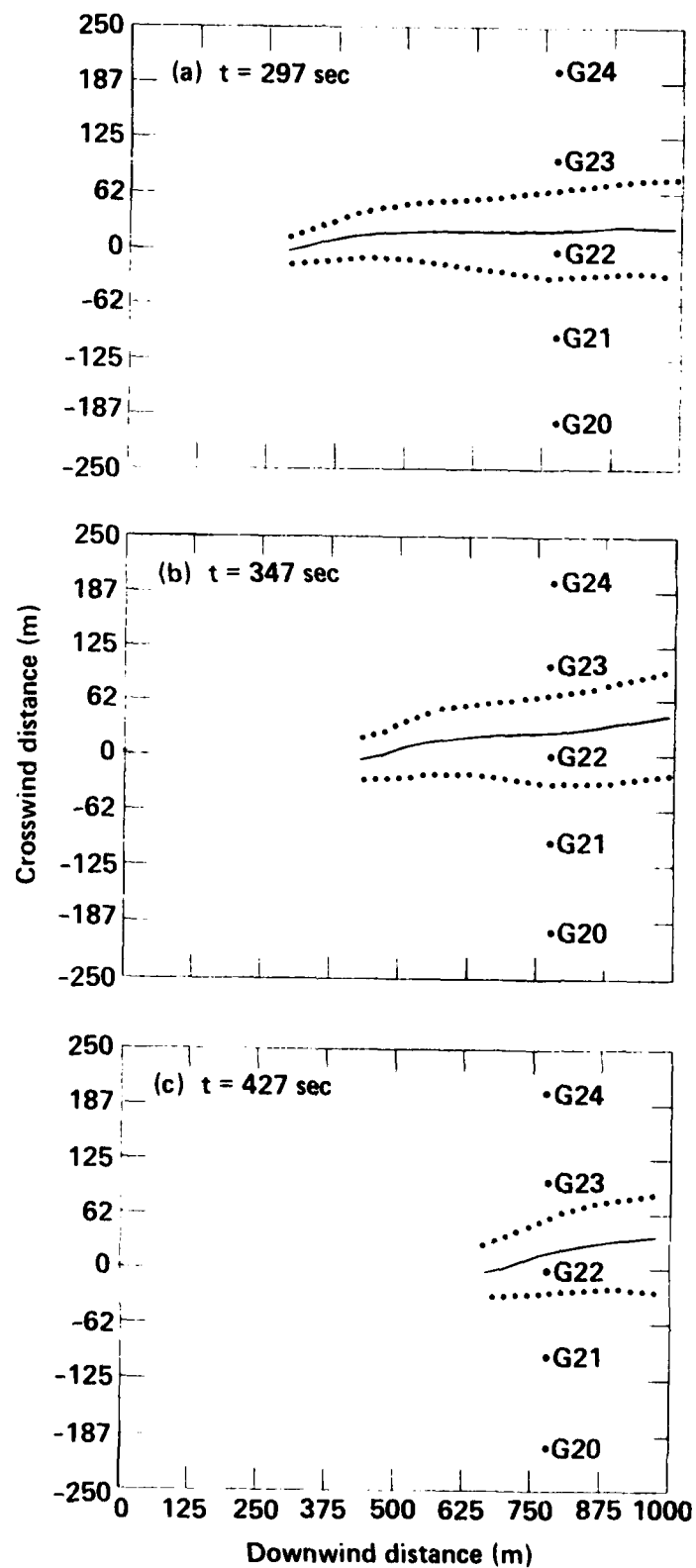


FIGURE 12. Eagle 3 Cloud Centerline Trajectories

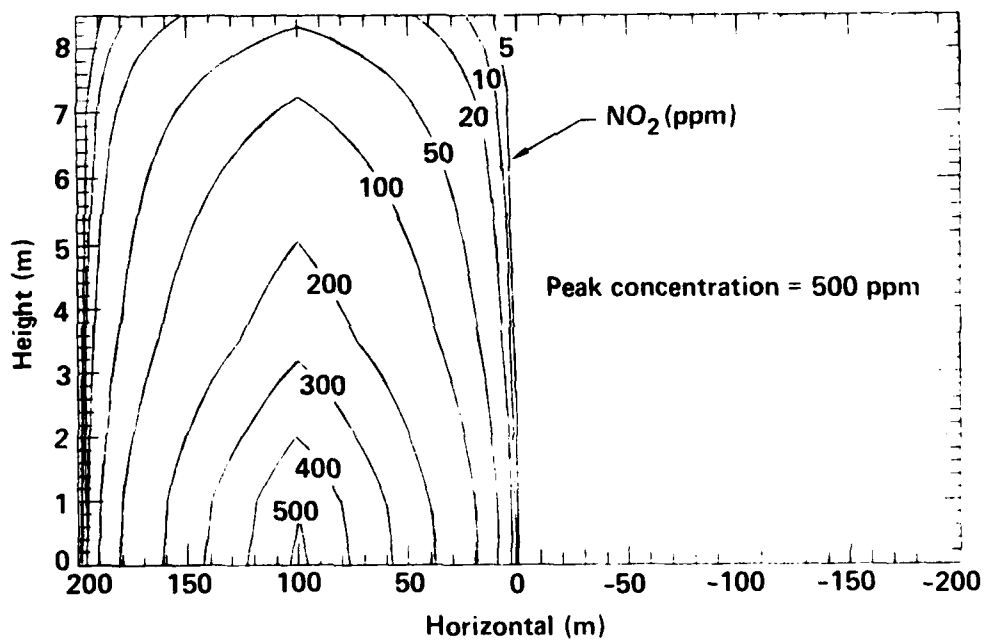


FIGURE 13. Eagle 3 Crosswind  $\text{NO}_2$  Concentration Contours at  $t = 300$  seconds  
(785 meters downwind)

Eagle 3 data of Figure 13. This is just another way of interpolating between the measured concentration values, which consist of three data points at Station G23 ( $z = 1, 3.5, 8.5$  meters), plus the knowledge that the concentration at the two adjacent stations (G22, G24) was less than the minimum detectable level of the sensors ( $< 1$  ppm).

The Gaussian equivalent cross section of the data of Figure 13 is shown in Figure 14. These contours were generated by using the measured peak concentration (500 ppm) and adjusting the standard deviations ( $\sigma_y, \sigma_z$ ) in the y and z dimensions until the two data sets (Figures 13 and 14) were as similar as possible. An exact match is not possible due to the difference between the linear interpolation and the Gaussian formulation, however there is no way of knowing which of the two is the more accurate representation of the true cloud cross section. The cross section dimensions of Figure 14 are  $\sigma_y = 35$  meters and  $\sigma_z = 3.8$  meters.

Use of the Gaussian cross-section distribution allows one to easily calculate the mass flux represented by Figure 14. This entails integration of the product of the local vapor density and windspeed over the entire y-z plane. The result for the Eagle 3 data of Figure 14 is 90.4 kilograms/minute, or 22 percent of the source strength estimate of 410 kilograms/minute. The missing 78 percent of the mass flux array may be attributed to the missing NO and HNO<sub>3</sub> concentrations, the fact that the measured NO<sub>2</sub> concentrations of station G23 may not be those of the cloud centerline (peak values), or that the actual concentration distribution is not truly Gaussian in shape. As determined by the mist formation analysis of Section III B, the HNO<sub>3</sub> and NO components made up roughly half of the cloud content at 25 meters. If this fraction were maintained downwind, then of the missing 78 percent, about 22 percent could be attributed to the missing HNO<sub>3</sub> and NO, and 56 the remaining percent to the off-center line underestimate of the peak concentration. For the cloud crosssection dimensions of Figure 14 and the total Eagle 3 source strength of 410 kilograms/minute, a peak NO<sub>2</sub> concentration of 2275 ppm would be obtained. This calculated peak concentration value, based on the calculated source strength and the inferred cloud size and shape, provides a second estimate of the actual peak concentration at 785 meters and will be used in evaluating the dispersion models. The range in peak concentration from 500 ppm to 2275 ppm is essentially an estimate of the uncertainty in the actual value.

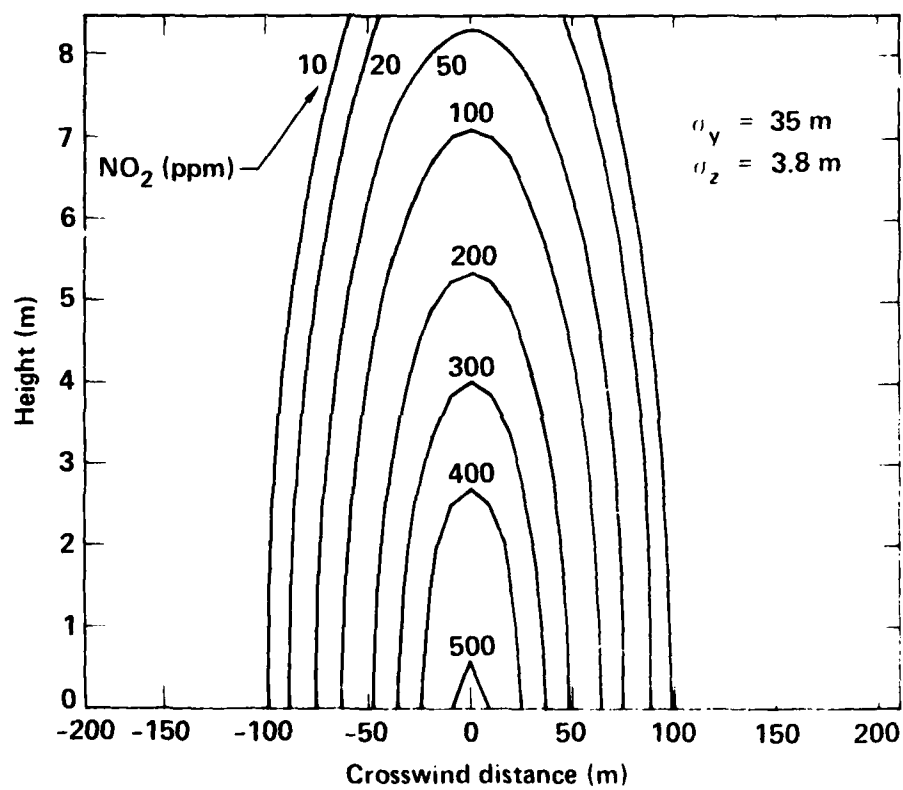


FIGURE 14. The Gaussian Equivalent Crosswind Concentration Distribution for the Eagle 3 Data at 785 meters

## 2. The Eagle 6 Test

A similar analysis of the Eagle 6  $\text{NO}_2$  data at 785 meters was also performed. The lack of knowledge as to the cloud composition ( $\text{NO}$ ,  $\text{HNO}_3$ ,  $\text{NO}_2$ ) and the cloud centerline location is the same in this case as for the Eagle 3 case. A superposition of the  $\text{NO}_2$  concentration data recorded at 785 meters during the passage of the Eagle 6 cloud is shown in Figure 15. As can be seen, from its initial arrival time of  $t = 170$  seconds to almost  $t = 400$  seconds, the cloud meandered between stations G21 and G22. The wind-field centerline trajectory plots for the Eagle 6 test are shown in Figure 16. These results also show the meander of the cloud, but indicate that the centerline favored station G22. At  $t = 400$  seconds the cloud passed across G22 with a small concentration being observed at G23 (Figure 15). Fortunately, this occurred just prior to the arrival of the large vapor puff generated by the nitrogen purge of the spill system. The choice of the time of the appropriate Eagle 6 cloud conditions was taken to be  $t = 430$  seconds. The crosswind  $\text{NO}_2$  concentration contours at this time are shown in Figure 17. As in the case of the Eagle 3 test, the peak concentration of Figure 17 (315 ppm) should be considered as a minimum value due to the missing  $\text{NO}$  and  $\text{HNO}_3$  contributions and the uncertainty in the cloud centerline location.

An equivalent Gaussian cross section was also created for the Eagle 6 data of Figure 17, however, the contour match was more difficult in this case due to the momentary lift-off of the cloud which occurred during this test. The Gaussian equivalent contours are shown in Figure 18 where the best fit was obtained for  $\sigma_y = 35$  meters and  $\sigma_z = 7.6$  meters. The  $\text{NO}_2$  mass flux for this case was 190 kilograms/minute, or about 55 percent of the source strength estimate. If we assume that about half of the mass cloud is in the form of  $\text{HNO}_3$  and  $\text{NO}$ , then very little of the mass loss error of the Eagle 6 data is due to the off-centerline underestimate of the peak concentration. This is consistent with the windfield centerline trajectory analysis. Just as was done with the Eagle 3 mass flux results, a second estimate for the Eagle 6 peak concentration can be made by using the total source strength of 344 kilograms/minute and the equivalent Gaussian cross section. This approach yields a peak concentration of 575 ppm. Therefore, the model predictions for the Eagle 6 spill will be compared to concentrations in the range of 315 to 575 ppm, where the upper limit accounts for the large-scale meander and the mass loss due to the unrecorded  $\text{NO}$  and  $\text{HNO}_3$ .

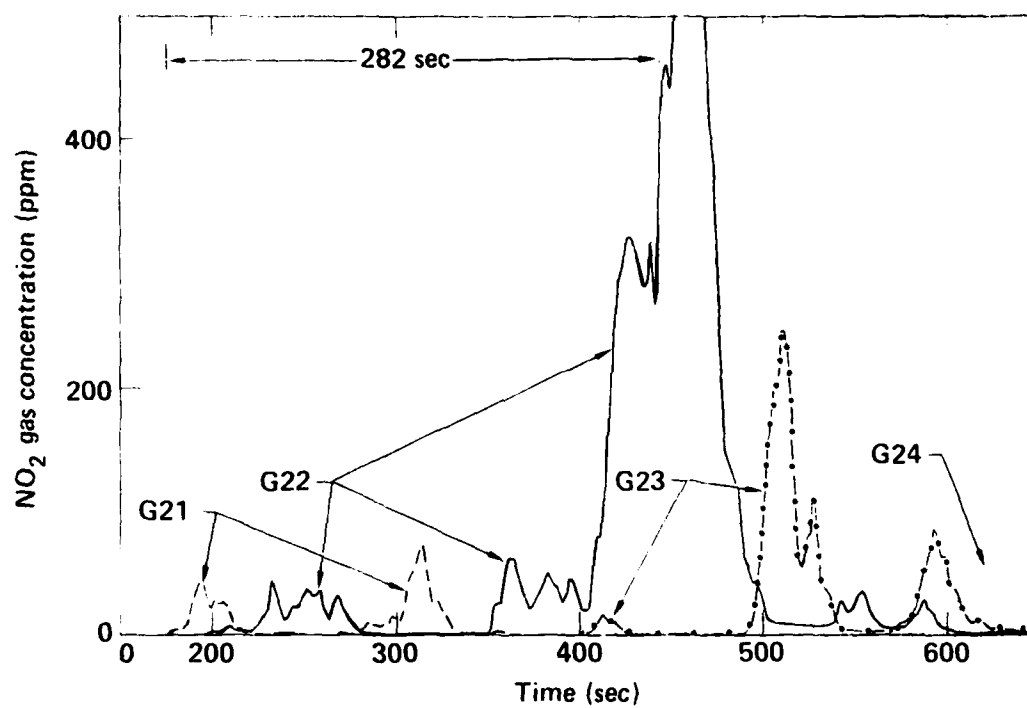


FIGURE 15. The Eagle 6 NO<sub>2</sub> Concentration (1 meter high, 785 meters downwind)



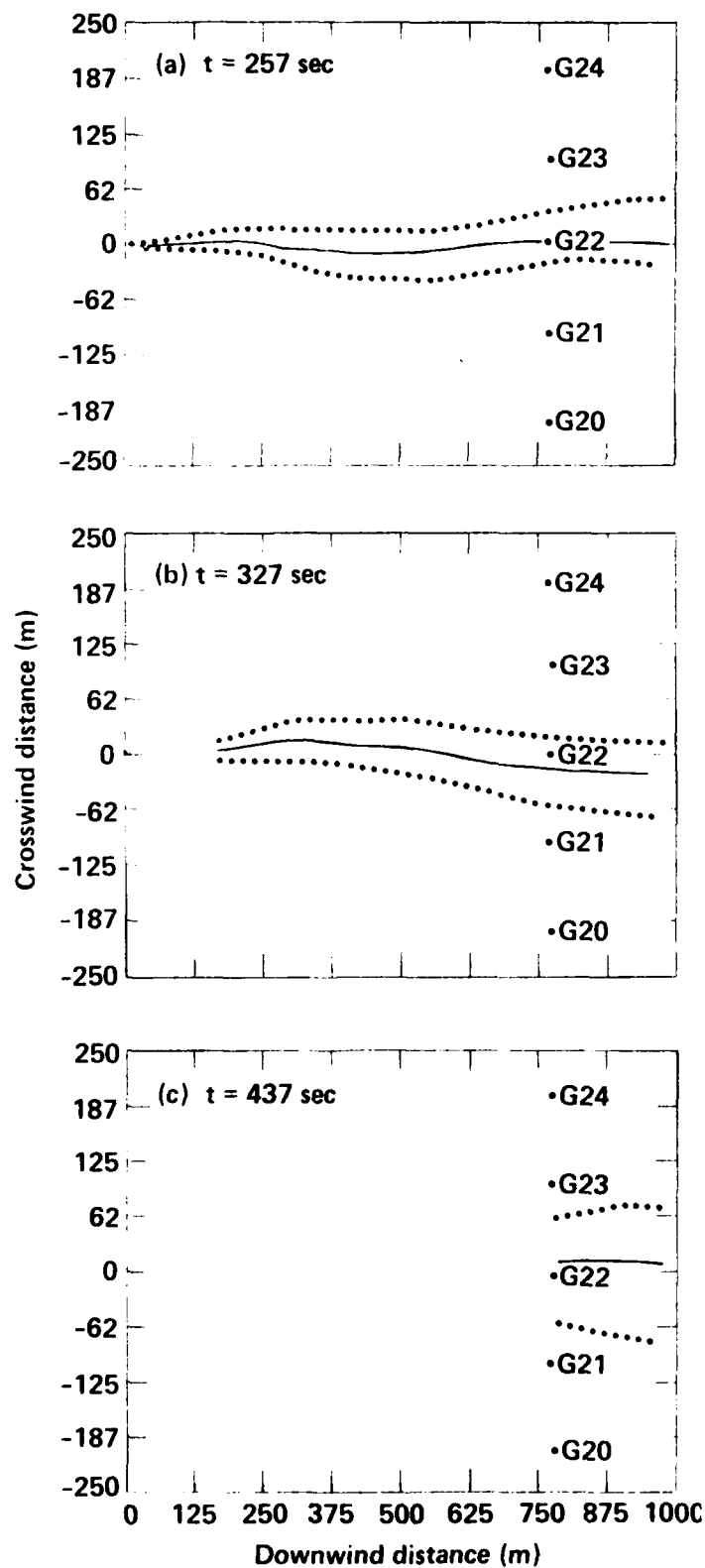


FIGURE 16. Eagle 6 Cloud Centerline Trajectories

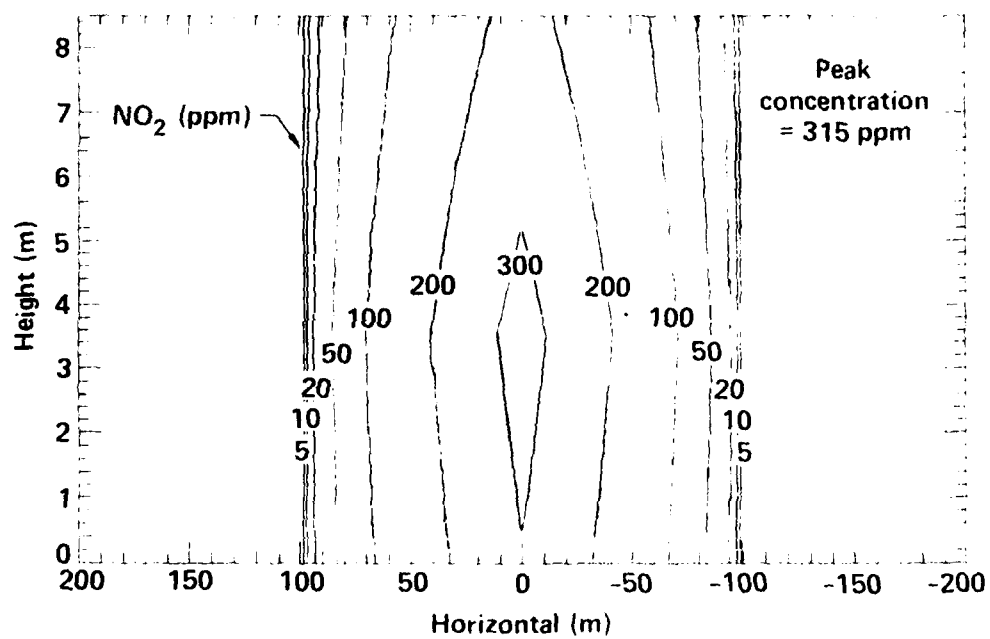


FIGURE 17. Eagle 6 Crosswind NO<sub>2</sub> Concentration Contours at t = 430 seconds (785 meters downwind)

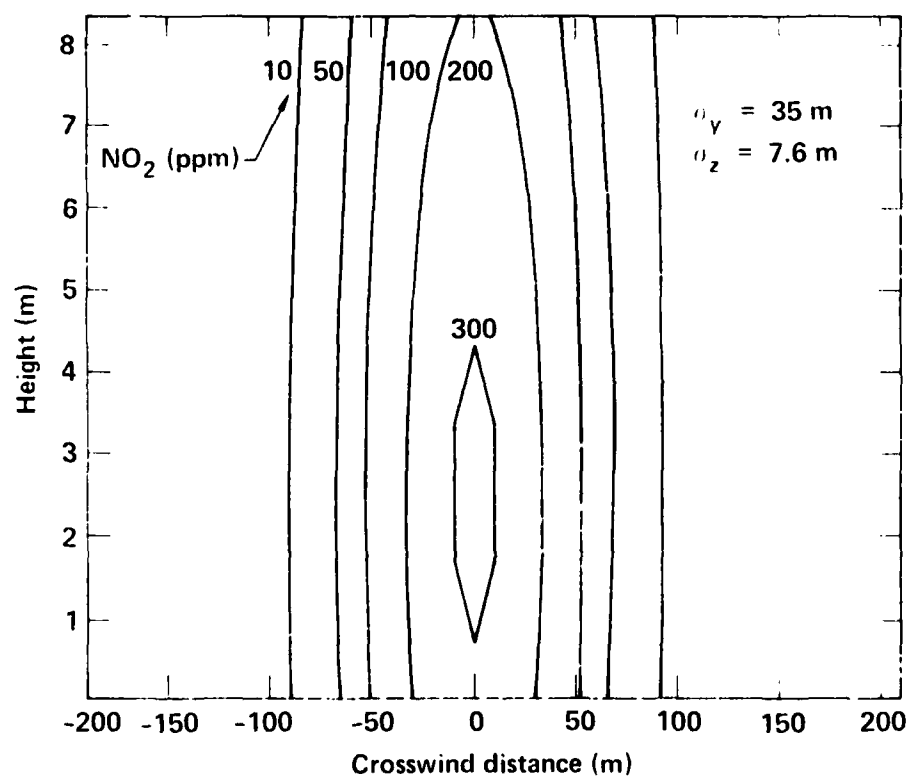


FIGURE 18. The Gaussian Equivalent Crosswind Concentration Distribution for the Eagle 6 Data at 785 meters

## B. COMPARISON OF DATA WITH DISPERSION MODEL PREDICTIONS

The primary purpose of the Eagle test series was to demonstrate the heavy-gas dispersion aspect of large-scale releases of  $\text{N}_2\text{O}_4$  vapors. The denser-than-air character of a heavy-gas cloud affects its subsequent dispersion in two main ways. The greater inertia of the heavy gas tends to reduce the rate of turbulent mixing from that of a trace gas, and thereby reduces the growth of the cloud. The greater density of the cloud produces a gravity flow or slumping which tends to reduce the cloud height and increase its width. These aspects of dense-gas dispersion have been previously recognized and the deviation of heavy-gas dispersion results from trace-gas dispersion model predictions has been published for a number of cases (Reference 27). In the following section, four simple Gaussian dispersion models will be briefly described, and then compared with the results of the Eagle 3 and Eagle 6 tests.

For the convenience of the reader, a summary (Table 10) of the model/data comparison results is presented in Section C.

### 1. The OB/DG Model

In late 1960, the Air Force conducted a series of dispersion tests (Reference 1) at Cape Kennedy, Florida (Ocean Breeze) and at Vandenberg AFB, California (Dry Gulch). These tests involved the release and detection of a zinc sulfide tracer. A total of 185 tests were performed under a wide range of atmospheric conditions. All of the data of the OB/DG tests were normalized and correlated to a simple diffusion prediction equation, the OB/DG model. This simple model predicted 75 percent of the cases to within a factor of two of the measured values. The model expresses the peak inhalation (1.5-meter-high)  $\text{NO}_2$  concentration  $C_p$  (ppm) as a function of source strength  $Q$  (kilograms/minute), the downwind distance  $x$  (m), the standard deviation in the horizontal wind direction  $\sigma_\theta$  (degrees), and the temperature difference  $\Delta T$  ( $^\circ\text{C}$ ) of the atmospheric boundary layer between the heights of 16.46 meters (54 feet) and 1.83 meters (6 feet), i.e.,

$$C_p = 17.15 Q x^{-1.96} (1.8 \Delta T + 10)^{4.33} \sigma_\theta^{-0.506}. \quad (14)$$

Two important measurements are required for Equation (14),  $\sigma_\theta$  and  $\Delta T$ . The  $\sigma_\theta$  values used in the generation of the OB/DG model were calculated from data obtained at a height of 3.66 meters which were smoothed by a 15-second interval, sliding average scheme to remove the high frequency fluctuations. The standard deviation of the smoothed horizontal wind data was then calculated for a period of time equal to the time of the tracer release, plus the time to travel to the measurement stations at the mean windspeed. The same process was used for calculating the Eagle 3 and Eagle 6  $\sigma_\theta$ 's used in Equation (14), the only difference being the measurement height, which was 3.36 meters in our case. Consequently, the  $\sigma_\theta$ 's used in Equation (14) are different from those given in Table 1.

No special data processing was reported (Reference 1) concerning the  $\Delta T$  data of Equation (14). The  $\Delta T$  values used in Equation (14) for the Eagle 3 and Eagle 6 spill conditions were obtained from 3-minute averages commencing at the initiation of the spill ( $t = 0$ ). To more closely represent the specified heights of 1.83 and 16.46 meters, the four measurement levels of the Eagle meteorological station (0.82, 2.46, 6.13, and 16.2 meters) were approximated using the standard variation of temperature with the natural logarithm of the height. A least squares, linear regression provides  $T_*$ , which may be used to interpolate for the temperature at the 1.83- and 16.46-meter levels.

The results of the OB/DG predictions are compared to the measured  $\text{NO}_2$  concentrations at 785 meters in Table 7. Also included in Table 7 are the  $\Delta T$  and  $\sigma_\theta$  values used in each case. It should also be noted that the OB/DG predictions are for a height above ground of 1.5 meters while the Eagle data was obtained at a height of 1 meter. However, this is not expected to change the results of Table 7 to any great extent. Obviously, the OB/DG model tends to underestimate the measured results by a very large amount.

TABLE 7. COMPARISON OF OB/DG PREDICTIONS WITH THE  
EAGLE TEST RESULTS AT 785 METER

<u>Test</u>	<u><math>\sigma_\theta</math> (deg)</u>	<u><math>\Delta T</math> (°C)</u>	<u>OB/DG <math>C_p</math> (ppm)</u>	<u>Measured <math>C_p</math> (ppm)</u>
Eagle 3	6.88	+0.422	165	500* -2275 <sup>+</sup>
Eagle 6	6.25	-0.460	73	315* - 575 <sup>+</sup>

\*Measured

<sup>+</sup>Calculated from source strength using  $C_p = \dot{m}_s / \pi \rho_v \sigma_y \sigma_z u$ .

## 2. The Pasquill-Hanna Gaussian Plume Model

The Gaussian, or normal, distribution function provides a general solution to the Fickian diffusion equation (Reference 28), and with the proper expression for the mean-square particle diffusion, forms the basis for most of the practical plume diffusion models currently in use. The steady-state Gaussian Plume model provides a general description of average plume diffusion because of the essentially random nature of atmospheric turbulence. Experimental diffusion studies by Hay and Pasquill (Reference 29), Cramer (Reference 30), and Barad (Reference 31) indicate that the Gaussian Plume formula has a wide area of practical applicability in the field of atmospheric dispersion.

The steady-state Gaussian Plume dispersion formula for releases located at ground level is

$$C_v = \frac{\dot{m}_s}{\pi \rho_v \sigma_y \sigma_z u} \exp - \frac{y^2}{2\sigma_y^2} - \frac{z^2}{2\sigma_z^2} \quad (15)$$

where  $C_v$  is the volume fraction of the dispersing gas,  $\dot{m}_s$  is the source strength,  $\rho_v$  is the vapor density at the ambient temperature and pressure,  $u$  is the average windspeed, and  $\sigma_y$  and  $\sigma_z$  are the one-sigma values of the concentration distribution in the  $y$  (crosswind) and  $z$  (vertical) dimensions. The values of  $\sigma_y$  and  $\sigma_z$  are generally expressed as functions of  $x$  (downwind distance) and depend on the atmospheric stability in effect at the time of the release.

The plume-spreading parameters which will be used in Equation (15) for comparison with the Eagle test results are listed in Table 8 according to the Pasquill turbulence types. These equations were obtained from Hanna, et al. (Reference 25) and are recommended for open-country conditions where 100 meters <  $x$  < 10 kilometers.

We must next decide which of the Pasquill stability types of Table 8 correspond to the Eagle 3 and Eagle 6 spill conditions. The relationships between the Pasquill types and  $\sigma_\theta$  are given in Table 9 (Reference 25). Whereas the OB/DG model varies continuously with  $\sigma_\theta$  and  $\Delta T$ , the Gaussian

Plume model is characterized by six distinctive categories. The  $\sigma_\theta$  of Table 9 are for a height of 10 meters, whereas the measured values of the Eagle tests (Table 1) were obtained at a height of 12 meters. According to Mitchell (Reference 32), there should be little difference between  $\sigma_\theta$ 's measured at 10 and 12 meters.

TABLE 8. PLUME-SPREADING PARAMETERS FOR OPEN-COUNTRY TERRAIN  
AND 100 METERS  $< x < 10$  KILOMETERS

<u>Pasquill type</u>	<u><math>\sigma_y</math> (m)</u>	<u><math>\sigma_z</math> (m)</u>
A	$0.22 \times (1 + 0.0001 x)^{-1/2}$	$0.20 x$
B	$0.16 \times (1 + 0.0001 x)^{-1/2}$	$0.12 x$
C	$0.11 \times (1 + 0.0001 x)^{-1/2}$	$0.08 \times (1 + 0.0002 x)^{-1/2}$
D	$0.08 \times (1 + 0.0001 x)^{-1/2}$	$0.06 \times (1 + 0.0015 x)^{-1/2}$
E	$0.06 \times (1 + 0.0001 x)^{-1/2}$	$0.03 \times (1 + 0.0003 x)^{-1}$
F	$0.04 \times (1 + 0.0001 x)^{-1/2}$	$0.016 \times (1 + 0.0003 x)^{-1}$

TABLE 9. RELATION BETWEEN WIND VARIABILITY ( $\sigma_\theta$ )  
AND PASQUILL STABILITY CLASS

<u>Stability Class</u>	<u><math>\sigma_\theta</math> Range (deg)</u>
A	$> 22.5$
B	$17.5 - 22.5$
C	$12.5 - 17.5$
D	$7.5 - 12.5$
E	$3.75 - 7.5$
F	$< 3.75$

There is also the choice of the time period over which to average the  $\sigma_\theta$  data. This is generally taken to be a 1-hour interval (Reference 33) so as to be compatible with the conventional Gaussian Plume formulation which includes the effects of large-scale cloud meander. The choice of this averaging time period can make a difference in the stability category as demonstrated in Figure 19, which shows the variation of  $\sigma_\theta$  with averaging time period for the Eagle 3 and Eagle 6 tests. Had we chosen an averaging time period of 10 to 25 minutes, then according to Table 9, both test conditions

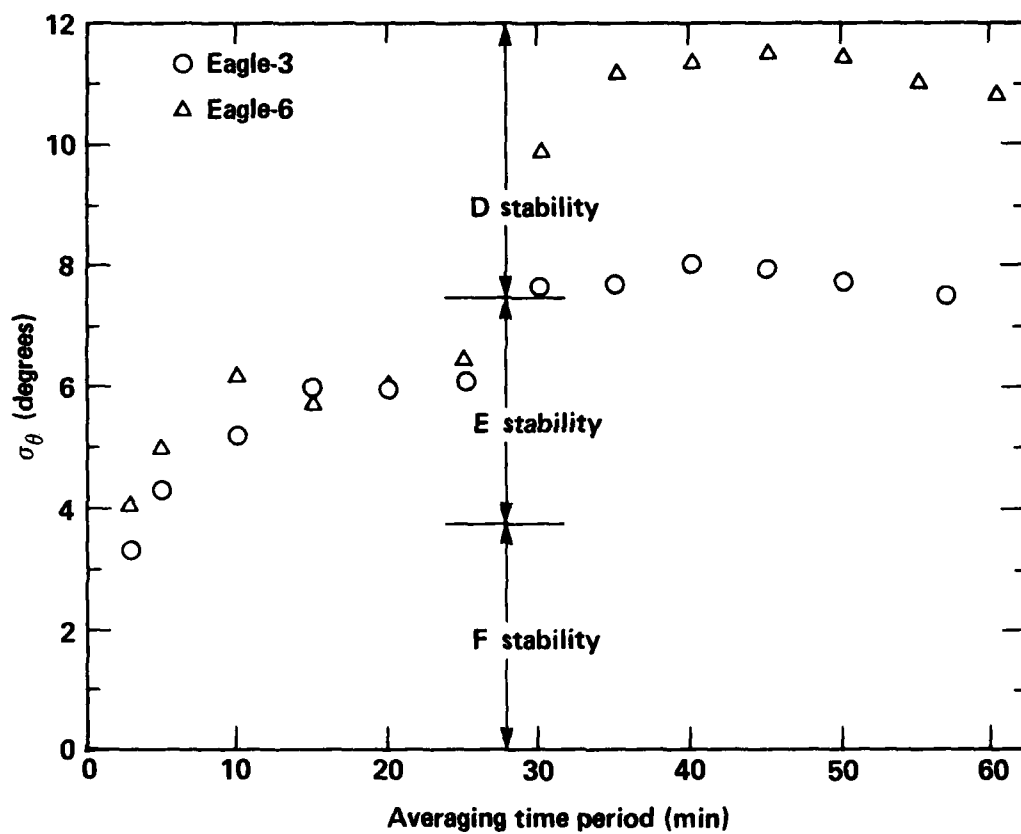


FIGURE 19. Variation of  $\sigma_\theta$  at 12 meters with Averaging Time Period for the Eagle 3 and Eagle 6 Tests



were essentially equal ( $\sigma_\theta = 6^\circ$ ) and of Class E. However, a 1-hour averaging time indicates that the two tests were somewhat different, but both classified as category D.

It should be noted that the correspondence between the measured  $\sigma_\theta$  and the Pasquill stability type is not the only way of determining the choice of stability. Relationships with Richardson number, Monin-Obukhov stability length and surface roughness do also exist (References 33, 34). While there is some general agreement between all of these parameters and the Pasquill stability class, the relationships may not hold for specific terrain and atmospheric conditions. For instance, as mentioned above, the 1-hour averaged  $\sigma_\theta$  values for Eagle 3 and Eagle 6 (Table 1) indicate that both would be Class D; however, the Richardson numbers indicate that Eagle 3 is in the stable regime (Class E,  $R = +0.37$ ), while Eagle 6 ( $R = -1.216$ ) should be in the unstable (Class B) regime. It is felt that the wind variability is the more fundamental physical quantity responsible for the dispersion process, hence the choice of the  $\sigma_\theta$  - Pasquill stability class relationship.

Using the measured windspeeds and source strengths, a vapor density ( $\rho_v$ ) of 1.72 kilograms/m<sup>3</sup>, and a stability class of D, the Gaussian Plume model (Equation 15) gives us a centerline ( $y = 0$ ,  $z = 1$  meter), concentration at  $x = 785$  meters of 163 ppm for Eagle 3 and 89 ppm for Eagle 6. The corresponding plume-spreading parameters are  $\sigma_y = 60.5$  meters, and  $\sigma_z = 31.9$  meters in each case. The predicted crosswind concentration distributions for both tests are shown in Figure 20.

We see that the Pasquill-Hanna Gaussian Plume model predicts about the same concentrations as the OB/DG model, and underestimates the measured values at 785 meters by at least a factor of four. Even if the highest stability class were used, class E, the predicted peak concentration at  $x = 785$  meters would be 364 ppm for Eagle 3 and 199 ppm for Eagle 6, still well below the recorded value. Once again, the reader is reminded that the peak recorded concentration for Eagle 3 (500 ppm) and Eagle 6 (315 ppm) are only minimum values due to uncertainties in the location of the cloud centerline and the missing contribution of the  $\text{HNO}_3$  and NO concentrations. The

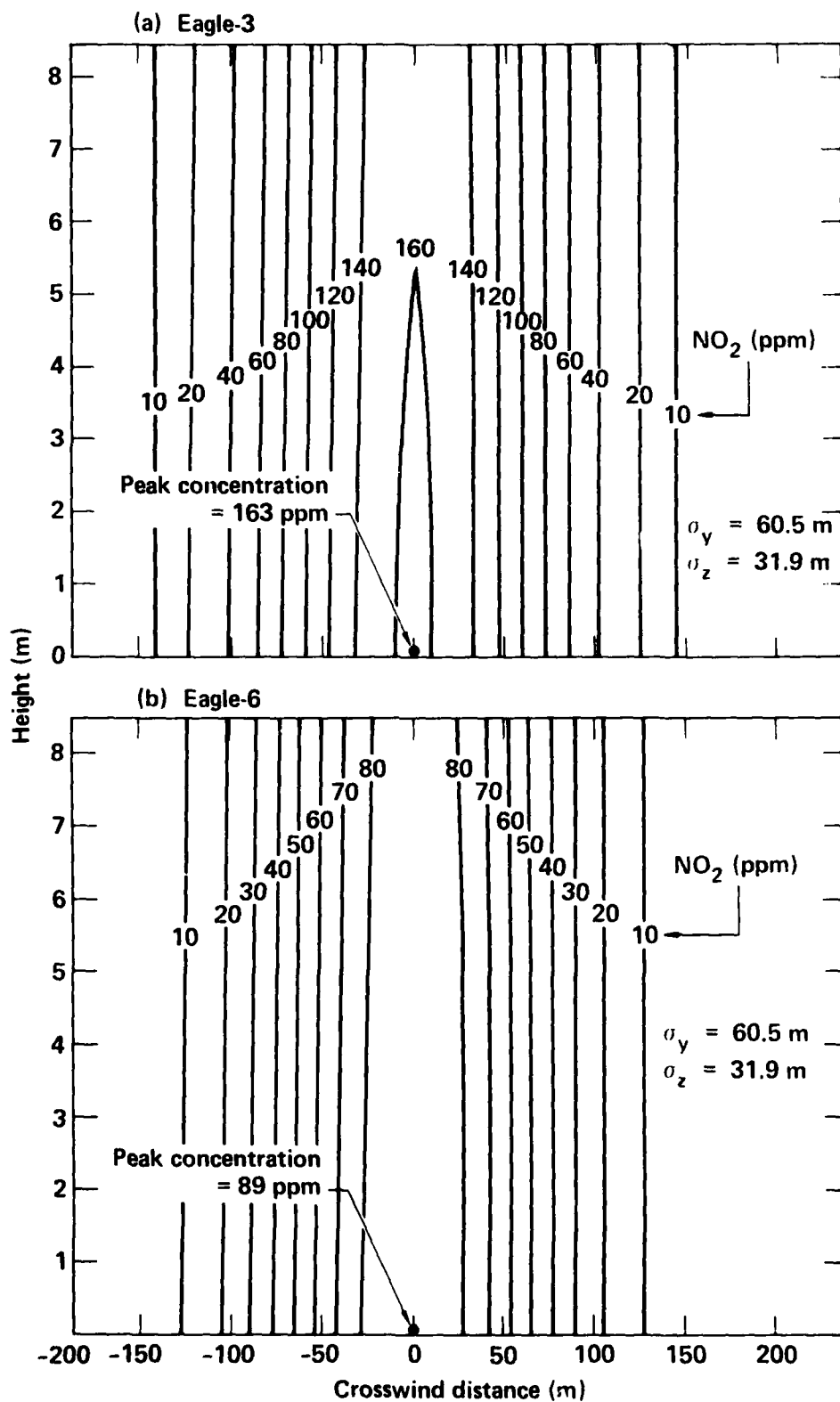


FIGURE 20. Eagle 3 and Eagle 6 Crosswind Concentrations as Predicted by the Gaussian Plume Model

equivalent Gaussian cross-section source strength calculations (Section IV A) indicate peak concentrations of 2275 and 575 ppm, respectively. A concentration contour plot of the Pasquill-Hanna Gaussian Plume cross section at  $x = 785$  meters is shown in Figure 20.

### 3. The Shell Dispersion Model

The Shell dispersion model is the dispersion portion of the Shell SPILLS model (Reference 17) and was run for the Eagle 3 and Eagle 6 conditions by Bruce Kunkel (AFGL). This model is based on Gaussian Puff diffusion principles which incorporate essentially the same assumptions as used in the Gaussian Plume model (Section IV B 2). However, the puff model can treat temporal variations in the source strength by approximating continuous releases with a series of small, discrete puffs. Each puff is treated as a symmetrical cloud of gas which is advected according to the windspeed and direction and is dispersed by atmospheric mixing. The cloud-spreading parameters ( $\sigma_y$ ,  $\sigma_z$ ) are the same as in the Gaussian Plume model, and therefore are functions of the downwind distance and the atmospheric stability class. The Shell Dispersion model assumes the dispersion along the direction of cloud movement ( $\sigma_x$ ) is equal to  $\sigma_y$ , and uses the spreading formulation of Turner (Reference 35). The model also allows for inversion layer effects; however, this is not an important feature for the Eagle series model/data comparisons. For steady state conditions, the Gaussian Puff model should give the same results as the Gaussian Plume model. For the Eagle 3 and Eagle 6 cases, the puffs were generated at a rate of one per second.

The Shell Dispersion model calculation for the Eagle 3 case gives a concentration of 199 ppm at  $x = 785$ ,  $y = 0$ , and  $z = 1$  meter. For the case of Eagle 6, the prediction is 112 ppm. The stability category in both cases was taken to be neutral (D). These results were for times after the beginning of the steady release of 17 and 20 minutes, respectively. These are adequate time intervals for steady-state conditions to be achieved at 785 meters for both the Eagle 3 and Eagle 6 tests. Consequently, the Shell Dispersion results (199 and 112 ppm) are quite similar to the Gaussian Plume results of the previous subsection (163 and 89 ppm). The small discrepancy has to do with the choice of plume-spread parameters, which for D stability are  $\sigma_y = 56$

meters and  $\sigma_z = 27$  meters from Turner (Reference 35), as opposed to  $\sigma_y = 60.5$  meters and  $\sigma_z = 31.9$  meters from Briggs (Reference 25).

#### 4. The CHARM Model

The Complex Hazardous Air Release Model (CHARM)<sup>®</sup> is a combination source strength and dispersion model, with associated software, developed by the Radian Corp., Austin, Texas. The model is available as a turn-key software/hardware system which provides the user with both tabular and graphic information. The system handles several different spill scenarios of both a transient and continuous nature, may be preprogrammed with local terrain data, and currently has built-in capability to handle 57 different chemicals. A special version of CHARM<sup>®</sup> capable of handling  $N_2O_4/NO_2$  spills and dispersion has been developed for Tyndall AFB, Engineering and Services Laboratory.

The most appropriate source strength module of CHARM<sup>®</sup> for comparison with the Eagle spill results is the instantaneous liquid release. This portion of the model is identical to the Shell evaporation model described in Section III E 2. The vapor-dispersion portion of the model is of the Gaussian Puff variety which divides the total amount released into a number of smaller amounts, each of which is treated as a separate release. For heavier-than-air vapors released at ground level, CHARM<sup>®</sup> initially invokes the "pancake" dispersion model of Eidsvik (Reference 37), followed by a Gaussian Puff calculation using the cloud spreading parameters of Reference 38. The transition between the Eidsvik and the Gaussian Puff models occurs when the average cloud density is within 1 percent of the ambient air density.

The Tyndall AFB  $N_2O_4/NO_2$  version of the CHARM<sup>®</sup> model was exercised for the Eagle 3 and the Eagle 6 test conditions by Mark Eltgroth (Environmental Inc.) under contract to RADIANT Corp. In its normal mode of operation, the source strength and dispersion portions of CHARM<sup>®</sup> are directly coupled. Therefore, to evaluate the dispersion portion of the model independently, the source strength portion was adjusted to produce the desired Eagle 3 and Eagle 6 results, 410 and 344 kilograms/minute, respectively. The CHARM<sup>®</sup> predictions at 785 meters for Eagle 3 were 220 ppm ( $\sigma_y = 60.5$  meters,

$\sigma_z = 23.6$  m), and for Eagle 6 were 127 ppm ( $\sigma_y = 58.7$  meters,  $\sigma_z = 23.2$  m). These results are slightly higher than those of the Gaussian Plume and Shell model results discussed earlier. This is due to the reduction in cloud spreading as a result of the Eidsvik phase of the cloud dispersion, which for both of the Eagle cases lasted about 30 seconds.

Users of the CHARM<sup>®</sup> model will find that obtaining the cloud peak concentration at a specific downwind distance is not a standard output option. The aforementioned results required some interpolation calculations due to the nature of the Gaussian Puff phase of the CHARM<sup>®</sup> dispersion model. The model divides the steady-state source into 10 equal puffs over the duration of the spill, which for the case of the Eagle 3 and Eagle 6 tests resulted in puffs being emitted at 18- and 28-second intervals, respectively. Although these puffs do overlap as they disperse and are carried downwind, their separation is of sufficient magnitude to produce concentration fluctuations in the downwind direction on the order of 20 percent. The CHARM results presented in this report are the result of calculations that "smooth out" these downwind concentration fluctuations so as to represent true steady-state cloud conditions.

### C. SUMMARY OF DISPERSION RESULTS

The NO<sub>2</sub> concentration results from the Eagle 3 and Eagle 6 tests have been compared with the predictions of the OB/DG model (Reference 1), Gaussian Plume model (Reference 25), Shell dispersion model (Reference 17), and the CHARM<sup>®</sup> model (Reference 26). A summary of these comparisons is given in Table 10. The model predictions are compared to the peak measured concentration at 785 meters, and the cloud cross section width ( $\sigma_y$ ) and height ( $\sigma_z$ ) determined from the Gaussian equivalent concentration distribution as explained in Section IV A. Also included in Table 10 are the peak concentrations determined by assuming a Gaussian cloud cross section and conservation of the source strength mass flux. These larger peak concentration estimates are reasonable attempts to account for the unmeasured NO and HNO<sub>3</sub> gases known to be in the cloud, plus the uncertainty of obtaining the peak cloud concentration due to large-scale plume meander.

TABLE 10. COMPARISON SUMMARY OF THE EAGLE TEST RESULTS  
AND DISPERSION MODEL PREDICTIONS

	Peak concentration (ppm)	$\sigma_y$ (m)	$\sigma_z$ (m)
EAGLE 3			
Test results			
Recorded	500		
Calculated <sup>+</sup>	<u>2275</u>	<u>35</u>	<u>3.8</u>
OB/DG	165	N/A	N/A
Gaussian Plume	163	60.5	31.9
Shell Dispersion	199	56.0	27.0
CHARM	220	60.5	23.6
EAGLE 6			
Test results			
Recorded	315		
Calculated <sup>+</sup>	<u>575</u>	<u>35</u>	<u>7.6</u>
OB/DG	73	N/A	N/A
Gaussian Plume	89	60.5	31.9
Shell Dispersion	112	56.0	27.0
CHARM	127	58.7	23.2

<sup>+</sup>Calculated from source strength using  $C_p = \dot{m}_s / \pi \rho_v \sigma_y \sigma_z u$ .

The comparison results indicate that all of the models examined substantially underpredict the measured peak NO<sub>2</sub> concentrations at 785 m. If we consider only the measured NO<sub>2</sub> results, the magnitude of the under-predictions range from a factor of about 4 for OB/DG to a factor of 2 for the CHARM<sup>®</sup> model. If, however, the Gaussian equivalent/mass conservation estimates are used for the Eagle 3 and Eagle 6 tests (2275 and 575 ppm, respectively) then all of the models underpredict the results by factors ranging from 5 to 14. The predicted cloud cross section dimensions, particularly the vertical dimension, are substantially larger than measured. Thus, the simple models predict more mixing than is observed to occur, primarily as a result of using trace-gas plume-spread parameters which are averaged over long time periods and which are independent of source strength and density effects.

## SECTION V

### CONCLUSIONS

The Eagle Series Analysis Report is divided into two main areas which deal with the topics of source strength (Section III) and vapor cloud dispersion (Section IV). A summary of this analysis is presented in each case (Sections III F and IV C). The general conclusions from this analysis are now presented for these two topics.

#### A. $N_2O_4$ SOURCE STRENGTH CONCLUSIONS

1. Large-scale test results are different from small-scale test results. Large, intense sources actually perturb the atmosphere, hence they have a different dependence on ambient conditions (windspeed, air temperature, insolation, stability class, etc.) than do small-scale sources.
2. The soil seepage effect on the Eagle source strengths was different from previous small-scale tests. There is no evidence in the Eagle test results that soil seepage reduces the source strength. Earlier small-scale tests indicated a reduction in source strength by factors of 3 to 5.
3. The final liquid temperature depends strongly on the liquid depth. A thin layer of  $N_2O_4$  will freeze ( $-11^\circ\text{C}$ ) even when supplied by warm fluid at up to 2000 kilograms/minute. Pool depths of 2 to 4 centimeters are warmer ( $0^\circ$  to  $5^\circ\text{C}$ ).
4. The internal energy (evaporative cooling) heat source is a major contributor to the source strength. This is especially true of unconfined spills, where evaporative cooling is responsible for more than half of the source strength.
5. Source strength models need improvement. Current models appear to overestimate the importance of windspeed and underestimate (or totally neglect) the importance of evaporative cooling, liquid depth, and soil seepage.

B.  $\text{N}_2\text{O}_4$  VAPOR DISPERSION CONCLUSIONS

1. Formation of a dense  $\text{HNO}_3$  mist may account for much of the downwind mass transport of large  $\text{N}_2\text{O}_4$  spills. This mist and its subsequent decomposition into NO and  $\text{HNO}_3$  vapors may greatly effect the dispersion characteristics of the cloud.
2. All of the simple models evaluated, underpredict the downwind gas concentration at 785 m by factors ranging from 2 to 14 depending on the various assumptions. The parameters used in the simple models are based on long-averaging times and therefore include large-scale meander effects. These are inappropriate for predicting short term concentrations. In addition, the cloud-spreading parameters for heavier-than-air releases are different than those of trace gases. Measured cloud height, for instance, is only 0.3 to 0.1 that predicted by the simple models.



# REFERENCES

1. Haugen, D.A., and J.J. Fuguay, The Ocean Breeze and Dry Gulch Diffusion Programs (Vols. 1 and 2), AFCRL-63-791, 1963.
2. Ohmstede, E.D., Dumbaule, R.K., and G.G. Worley, Ocean Breeze/Dry Gulch Equation Review, ESL-TR-83-05, AFESC, Tyndall AFB, FL, 1983.
3. McRae, T.G., R.T. Cederwall, H.C. Goldwire, Jr., D.L. Hipple, G.W. Johnson, R.P. Koopman, J.W. McClure, and L.K. Morris, Eagle Series Data Report, UCID-20063, Lawrence Livermore National Laboratory, Livermore, CA, 1984.
4. Giauque, W.F., and J.D. Kemp, J. Chem. Phys., Vol. 6, p. 40, 1938.
5. Nordstrom, R.J., and W.H. Shan, "A Spectroscopic Study of the  $\text{NO}_2\text{-N}_2\text{O}_4$  System by the Infrared Absorption Technique," J. Phys. Chem., Vol. 80, No. 8, p. 847, 1976.
6. Bingham, G.E., R.D. Kiefer, C.H. Gillespie, T.G. McRae, H.C. Goldwire, Jr., and R.P. Koopman, "A Portable, Fast-Response Multiwavelength Infrared Sensor for Liquefied Natural Gas Vapors," UCRL-84850, Rev. 1 (1982). Rev. Sci. Instrum., Vol. 54, No. 10, p. 135b, 1983.
7. Baker, J., The LGF Data Acquisition System, Lawrence Livermore National Laboratory, Livermore, Calif., UCID-19431, 1982.
8. McRae, T.G., H.C. Goldwire, Jr., and R.P. Koopman, "The Evaporation and Gaseous Dispersion of Large-Scale Releases of Nitrogen Tetroxide," UCRL-89687, presented at, 1984 JANNAF S&EPS, Annual Meeting, NASA White Sands Test Facility, May, 1984.
9. Goyer, G.G., "The Formation of Nitric Acid Mists," J. Colloid Sci., Vol. 18, p. 616-624, 1963.
10. England, C., and W.H. Corcoran, "Kinetics and Mechanisms of the Gas-Phase Reaction of Water Vapor and Nitrogen Dioxide," Ind. & Eng. Chem. Fundamentals, Vol. 13, p. 173, 1974.
11. Peters, M.S., and J.L. Holman, "Vapor and Liquid-Phase Reactions Between Nitrogen Dioxide and Water," Ind. & Eng. Chem., Vol. 47, p. 2536, 1955.
12. Chambers, F.S., Jr., and T.K. Sherwood, "Absorption of Nitrogen Dioxide by Aqueous Solutions," Ind. & Eng. Chem., Vol. 29, p. 1415, 1937.
13. Hilbers, C.E., Titan II Toxic Sources, BSD TR 65-97, Feb. 1963 (Available through DTIC as AD371799).
14. McNerney, J.L., D.E. Towson, and W.P. Henderson, Nitrogen Tetroxide Evaporation Rate Studies, EATM 511-1, Edgewood Arsenal, MD, Aug. 1966 (available through DTIC as AD488566).
15. Kunkel, B.A., A Comparison of Evaporative Source Strength Models for Toxic Chemical Spills, AFGL-TR-83-0307, Air Force Geophysics Lab., Hanscom AFB, MA., 1983.

16. Ille, G., and C. Springer, The Evaporation and Dispersion of Hydrazine Propellants from Ground Spills, CEEDO-TR-78-30, Tyndall AFB, FL, 1978.
17. Fleischer, M.T., Mitigation of Chemical Spills: An Evaporation/Air Dispersion Model for Chemical Spills on Land, Shell Development Co., Houston, TX, 1980.
18. Whitacre, C.G., and M.M. Myirski, Computer Program for Chemical Hazard Prediction, ARCSL-TR-82014, Army Chemical Systems Lab., Edgewood Arsenal, MD, 1982.
19. Clewell, H.J., A Simple Formula for Estimating Source Strengths from Spills of Toxic Liquids, ESL-TR-83-03, Tyndall AFB, FL, 1983.
20. Kahler, J.P., R.G. Curry, and R. A. Kandler, "Calculating Toxic Corridors," AWS/TR-80/003, Scott AFB, IL, 1980.
21. Perry, M.H. (Ed.), Chemical Engineer's Handbook, 3rd edition, McGraw-Hill Book Co., Inc., 1950.
22. Wilson, J.B., and J.E. Miles, "The Partial Pressures of Nitric Acid-Water Mixtures from 0°-20°C.," Trans. Faraday Soc., Vol. 36, p. 356, 1940.
23. Johnston, H.S., L. Foering, Y.S. Tao, and G.H. Messerly, "The Kinetics of the Thermal Decomposition of Nitric Acid Vapor," J. Amer. Chem. Soc., Vol. 73, p. 2319, 1951.
24. Koopman, R.P., R.T. Cederwall, D.L. Ermak, H.C. Gopldwire, Jr., W.J. Hogan, J.W. McClure, T.G. McRae, D.L. Morgan, H.C. Rodean, and J.H. Shinn, "Analysis of Burro Series 40-m<sup>3</sup> LNG Spill Experiments," J. Haz. Mat'l, Vol. 6, p. 43-83, 1982.
25. Hanna, S.R., G.A. Briggs, and R.P. Hoster, Handbook on Atmospheric Dispersion, DOE/TC-11223, DOE Technical Information Center, p. 102, 1982.
26. Description of the Radian Complex Hazardous Air Release Model (CHARM)<sup>®</sup> and Associated Micro-computer Based Systems, Radian Corp., Austin, TX, 1983.
27. Ermak, D.L., S.T. Chan, D.L. Morgan, and L.K. Morris, "A Comparison of Dense-Gas Dispersion Model Simulations with Burro Series LNG Spill Test Results," J. Haz. Mat'l, Vol 6, p. 129-160, 1982.
28. Sutton, O.G., Micrometeorology, McGraw-Hill Book Co., NY, 1953.
29. Hay, J.S., and F. Pasquill, "Diffusion from a Continuous Source in Relation to the Spectrum and Scale of Turbulence," Advances in Geometry, 6, p. 345-365, F.N. Frenkiel and P.A. Sheppard (Eds.), Academic Press, NY, 1959.
30. Cramer, H.E., "A Practical Method for Estimating the Dispersal of Atmospheric Contaminants," First National Conference on Applied Meteorology, Sec. C, p. 33-35, American Meteorological Society, Hartford, CO, 1957.

31. Barad, M.L. (Ed.), Project Prairie Grass: A Field Program in Diffusion, Geophysical Research Paper, No. 59, Vols. I and II, AFCRC-TR-58-235, Air Force Cambridge Research Center, 1958.
32. Mitchell, A.E., "A Comparison of Short-term Dispersion Estimates Resulting from Various Atmospheric Stability Classification Schemes," Atmos. Environ., Vol 16, p. 765-773, 1982.
33. Hanna, S.R., G.A. Briggs, J. Deardorff, B.A. Egan, F.A. Gifford, and F. Pasquill, "AMS Workshop on Stability Classification Schemes and Sigma Curves - Summary of Recommendations," Bull. Amer. Met. Soc., Vol 58, No. 12, p. 1305-1309, 1977.
34. Sedefian, L., and E. Bennett, "A Comparison of Turbulence Classification Schemes," Atmos. Environ., Vol 14, p. 741-750, 1980.
35. Turner, D.B., Workbook of Atmospheric Dispersion Estimates, U.S. Dept. of Health, Education and Welfare, Public Health Service Pub. No. 999-AP-26, (Rev., 1969.
36. Irwin, J.S., "A Theoretical Variation of the Wind Profile Power Law Exponent as a Function of Surface Roughness and Stability," Atmos. Environ. Vol 13, p. 191-194, 1979.
37. Eidsvik, K.J., "A Model for Heavy-Gas Dispersion in the Atmosphere," Atmos Environ., Vol 14, p. 769-777, 1980.
38. Bowers, J.F., J.R. Bjorklund, and C.S. Cheney, Industrial Source Complex Dispersion Model User's Guide. Vol. 1., E.P.A. Report No. EPA-450/4-79-030, U.S. Environmental Protection Agency, Research Triangle Park, N.C., 1979.

**END**

**FILMED**

**10-85**

**DTIC**